New insights into the reaction of tricalcium silicate (C<inf>3</inf>S) with solutions to the end of the induction period

Downloaded from: https://research.chalmers.se, 2026-04-05 13:27 UTC

Citation for the original published paper (version of record):
Huang, L., Tang, L., Gu, H. et al (2022). New insights into the reaction of tricalcium silicate (C<inf>3</inf>S) with solutions to the
end of the induction period. Cement and Concrete Research, 152.
http://dx.doi.org/10.1016/j.cemconres.2021.106688

N.B. When citing this work, cite the original published paper.

research.chalmers.se offers the possibility of retrieving research publications produced at Chalmers University of Technology. It covers all kind of research output: articles, dissertations, conference papers, reports etc. since 2004. research.chalmers.se is administrated and maintained by Chalmers Library

(article starts on next page)

Cement and Concrete Research 152 (2022) 106688

Contents lists available at ScienceDirect

Cement and Concrete Research

journal homepage: www.elsevier.com/locate/cemconres

New insights into the reaction of tricalcium silicate (C_3S) with solutions to the end of the induction period

Liming Huang [a,b,*,**], Luping Tang [b], Haitao Gu [a], Zhen Li [a], Zhenghong Yang [a,***]

[a] Key Laboratory of Advanced Civil Engineering Materials, Ministry of Education, Tongji University, Shanghai 201804, PR China
[b] Department of Architecture and Civil Engineering, Chalmers University of Technology, 41296 Gothenburg, Sweden

ARTICLE INFO

Keywords:
C_3S
Hydration
Induction period
Nucleation
Particle attachment

ABSTRACT

Although dissolution theory is widely used, in certain circumstance, it seems to be unable to explain the hydration of C_3S. In this article, more attention is paid to the nucleation of hydration products. We find that the precipitation of C-S-H is a nonclassical nucleation process. It starts with nucleation of primary particles and then grows by particle attachment. A sharp increase in the reaction rate after induction period may come from the accelerating growth rate of C-S-H instead of dissolution of etch pits. The duration of induction period relates to the size of primary floc. Potassium salts influence the primary globule floc size and mitigate the effect from Al. The pH impacts ion species in solution to affect the dissolution and precipitation. A hypothesis regarding the dissolution of C_3S and nucleation of C-S-H within the near-surface region may narrow the gap between dissolution theory and protective layer theory.

1. Introduction

The hydration of cement is a sophisticated process, but the research of it is of great significance for both practical and scientific interest. During the past decades, there were several reviews on the investigation of the hydration mechanism. Even though it has been studied for so many years, some problems remain unsolved or under argument for the hydration of some pure minerals. The hydration of C_3S has attracted considerable attention because it is the main constituent of ordinary Portland cement. Having a better understanding of its hydration is a critical step to unveil the mechanism of the cement hydration. A majority of the previous studies classified C_3S hydration into 5 regions as in [1], and Scrivener et al. [2] simplified this into 3 periods: I- up to the end of the induction period (IP); II- the main hydration peak; III- hydration after the main peak. Whether the reaction in period I is controlled by the formation of a protective layer covering the surface [3] or only the dissolution rate [4] is still hotly debated. The duration of period I and the reaction rate at this period would be affected by many factors, including intrinsic properties (particle size, doping of impure elements and annealing treatment) and external factors (inorganic salts, organic chemicals and temperature). Herein we present a short review on some interesting investigations about how these factors impact the hydration of C_3S or cement during the IP.

1.1. Particle size/specific surface area and annealing

The size of mineral particles has an impact on the reaction of C_3S during the IP. Costoya [5] performed a systematic work to assess the hydration of C_3S with different particle size distributions, ranging from 6 up to 240 μm. The lowest heat flow from the hydration of coarse particles is lower than that of the fine particles during IP, and the duration of the induction period (DIP) for the large particles is longer than the small ones. A higher specific surface area can shorten the DIP [6,7]. An annealing treatment of C_3S at 650 °C results in a longer IP without much influence on its particle size distribution. Some authors hold the opinion that the unannealed C_3S and the smaller particles had a higher dissolution rate during the IP due to a higher defects density on the surface [5,6,8]. However, the surface defects may have little effects on the dissolution rate of minerals such as calcite [9], silicates [10], and the annealed C_3S [11].

* Correspondence to: L. Huang, Department of Architecture and Civil Engineering, Chalmers University of Technology, 41296 Gothenburg, Sweden.
** Correspondence to: L. Huang, Key Laboratory of Advanced Civil Engineering Materials, Ministry of Education, Tongji University, Shanghai 201804, PR China.
*** Corresponding author.
E-mail addresses: limingh@chalmers.se (L. Huang), tjZHY92037@163.com (Z. Yang).

https://doi.org/10.1016/j.cemconres.2021.106688
Received 6 March 2021; Received in revised form 24 November 2021; Accepted 30 November 2021
Available online 7 December 2021
0008-8846/© 2021 The Authors. Published by Elsevier Ltd. This is an open access article under the CC BY license (http://creativecommons.org/licenses/by/4.0/).

1.2. Doping elements

The incorporation of trace elements and the annealing treatment of clinker induce polymorphs of C_3S [12,13]. C_3S in different crystal systems has a distinct hydration heat release rate to the end of the IP [14]. Triclinic crystal has the shortest IP while the monoclinic system has much longer IP. The doping of 2.5% Cr, Ni and Zn can stabilize the C_3S in T_2, T_2 and M_2 crystals, respectively, and M_2 C_3S doped with Zn has the longest IP [15]. Although C_3S doped with Cr and Ni are in the same crystal system, the reactivity presents evident differences. Monoclinic C_3S doped with excessive Cu prolongs the IP up to 250 h [16]. These effects may also result from the trace elements dissolved into the pore solution. Gineys et al. [17] noticed that Cu, Zn and Pb in the solution increased the duration of IP of cement hydration. Dietmar Stephan [18,19] reported that the incorporation of Mg, Al and Fe below 1% changed the crystal structure of C_3S, but they had little influence on the DIP and the hydration rate during the IP. Bazzoni [20] also found that doping of Mg and Zn had an impact on the main peak but it induced very limited effect on the DIP. Most of the published papers unilaterally connect the effect from doping to its influence on the dissolution rate of C_3S [21–25]. Its effect on nucleation and growth of hydration products deserves attention as well.

1.3. Water/binder ratio, inorganic and organic admixtures

Water plays a key role in the hydration of C_3S. According to [22], the water to binder ratio (from 0.4 to 0.97) has little effect on the IP of triclinic C_3S (henceforth noted as TC_3S) and cement. Recently, Naber et al. [23] reported that the water to C_3S ratio (w/c) may have some effects on the reaction rate up to 5 h. However, in their study the saturated $Ca(OH)_2$ (CH) solution was used and the reaction rate was indicated by ex-situ X-ray diffraction (XRD) and thermogravimetric analysis (TGA) of samples dried at 60 °C. The results from Brown et al. [24] indicated that the w/c hardly affects the Ca^{2+} concentration in the IP, which means that the increase of w/c will augment the dissolving amount of the solid ingredient to gain a critical supersaturation condition in this period.

Inorganic chemicals in the solution make impact on the DIP as well. The saturated $CaSO_4$ solution prolonged the DIP but $CaCl_2$ solution narrowed this period [25]. Many other soluble chlorides ($MgCl_2$, $NiCl_2$ and YCl_3) presented a reducing effect on the DIP. An interesting small peak occurred in the long IP (about 15 h) when C_3S was hydrated in a $CuCl_2/CuSO_4$ solution [26]. NaOH [27,28] and KOH [29] evidently shortened the DIP. A high alkalinity even induced the hydration process to get rid of the IP [30]. Some nanosized insoluble inorganics also presented a reduction in the DIP. It is recognized as a seeding effect not only on the hydration in IP but more evidently on the main hydration peak. C-S-H seeds (precipitated from aqueous solutions of sodium silicate and calcium nitrate) effectively shortened the IP of C_3S and cement hydration [31]. It is interesting that afwillite seed (prepared from C_3S hydration) evidently enhances the main peak but has little effect on the IP [32]. This implies that the effect from C-S-H seed on DIP can hardly be explained by providing nuclei to accelerate hydration. Nanosized $CaCO_3$ [33] and TiO_2 [34] shortened the IP and increased the lowest hydration rate from C_3S or cement in the IP.

Many organic admixtures that have strong complexation with Ca ions will prolong the IP, such as sucrose, tartaric acid and succinic acid [35]; lignosulfonates, glucose and sodium gluconate [36]; cellulose ethers [37]; D-glucitol, D-galactitol and D-mannitol [38]; and polycarboxylate polymers [39]. Some of these admixtures have weak influence on the dissolution kinetics of pure C_3S and even increase its dissolution rate, which can be deduced from the pore solution evolution in [38]. The popular explanation for the retarding effect from organic admixtures will be summarized in the next paragraph.

1.4. Limitation of current theories for the IP

The two most popular theories for explaining the rapid decrease in the heat release during early hydration are protective membrane and dissolution controlled by undersaturation. These theories are well summarized and distinguished in [2]. The dissolution theory may be better for explaining the emerge of the IP than the protective membrane, but it seems to be inapplicable for explaining the retarding effect of organic admixtures by only considering the relationship between dissolution rate and thermodynamic of bulk pore solution. This theory tries to explain the retarding effect by the reason that the ions or molecules adsorbed on the particle surface passivate the active sites and block the dissolution of defects, like dislocations outcropping on the surface, or point defects [4,40]. However, the dissolution rate is increased by some organic retarders as highlight in the above paragraph. Moreover, it is doubtful that the longer IP of the annealed C_3S can be explained by the dissolution theory, because the surface defects may have little effect on the dissolution rate of minerals. Therefore, it is more reasonable to ascribe the long DIP to the inhibition of the nucleation and growth of hydration products (Portlandite or C-S-H) induced by the admixtures [35,41–43]. This inhibiting effect will delay the starting time of the acceleration period to increase the IP.

This paper presented our study on the hydration of TC_3S with solutions, which started with deionized water and sulfuric acid. The preliminary results indicate that it is difficult to explain the hydration of C_3S with a high w/c by the dissolution theory. Therefore, we focused on a deep analysis on the interfacial nucleation of C-S-H and the dissolution etch pits on TC_3S surface with normal w/c. In the discussion section, we try to use a hypothesis to provide a holistic explanation for the hydration process from water contact to the end of the IP. The hydration evolution was monitored by an isothermal calorimetry test. The composition and morphology of hydration products were determined by XRD and scanning electron microscopy (SEM). GEMS simulation results supplied a significant information on the distribution of ion species in the pore solution.

2. Experiments and simulation

2.1. Materials and procedures

Triclinic C_3S is the same materials used in [29] with a purity of 98.57% and a specific surface area of 1.92 m^2/g. The particle size distribution is presented in Fig. 1. The majority of C_3S has a size smaller than 10 μm. The sulfuric acid solution (pH = 1 and 4) was diluted from the AR sulfuric acid (CAS:7664-93-9). All of the materials were preserved at 25 ± 1 °C before mixing. The hydration heat test of C_3S with very high solution/solid ratio was operated by mixing 0.1 g C_3S with 10 g (100/1) and 20 g (200/1) solutions in the ampere bottle, respectively, within 30 s before putting them into calorimeter channels. To get enough solid residue for the XRD test, the parallel experiments were

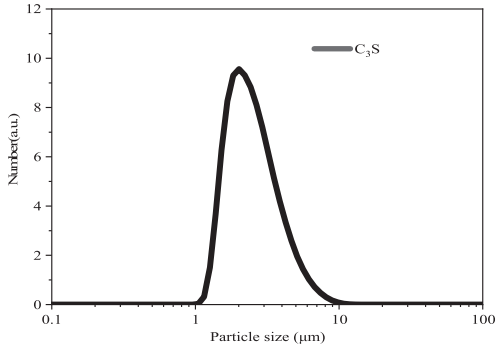

Fig. 1. Particle size distribution of C_3S powder.

carried out by using five times as much materials as in the calorimetry test. One more hydration experiment with a w/c of 600 was performed to check the dissolution of C_3S. All samples were only stirred at the initial mixing for about 1 min. After hydration for 4 h the solid residues were obtained by suction filtration and then cleaned with an adequate volume of isopropanol for three times to stop the hydration. The washed residues were vacuum dried at 40 °C for 48 h and then preserved in a sealed tube for XRD analysis.

Further experiments were carried out with a solution to C_3S ratio of 0.5 at 25 °C. The solutions include deionized water (TC_3S), 0.06 g/mL KOH solution (KH) and 0.06 g/mL K_2SO_4 solution (KS). The samples were stirred for 1 min in a glovebox with N_2 gas and then cured in the box before they were taken out to stop hydration. The hydration was stopped at 0.5 h for SEM analysis. The procedure for stopping the hydration and drying is the same as the high w/c system.

The cubic tricalcium aluminate (C_3A) purchased from DMT Materials Technology Co., Ltd. was used to replace a part of the C_3S to make a C_3S: C_3A mixture system (90%:10% by weight). The specific surface area of C_3A powder is 1.26 m^2/g. The hydration experiments of mixture system with deionized water, KH, and KS were performed with a solution to solid ratio of 0.5 at 25 °C in a glovebox. It was stopped at 4 h by immersing the samples into liquid nitrogen and then samples were quickly moved into a freeze-drying machine at −50 °C and 0.7 Pa for 3 days. The same procedure was used to stop the hydration of a reference sample (pure C_3S with deionized water).

2.2. Methods

The specific surface area of C_3A was measured by the same method applied to C_3S in [29]. The XRD of the hydration products was determined by a Rigaku International Corporation D/max 2550 VB3+/PC diffractometer (Cu Kα radiation). The measurements were conducted in the range of 5–45° (2θ) with a step of 0.05°, a counting time of 1 s/step, a tube voltage of 40 kV and a current of 100 mA.

The Au-plated hydration particles were detected by a Nova NanoSEM 450 scanning electron microscope. The accelerating voltage and beam current for the images were 10 kV and 0.5 nA, respectively.

The hydration heat release was tested by the TAM Air Isothermal Calorimeter from TA Instruments (TAM air C80, Thermometric, Sweden). The sample was only stirred within the initials 30 s and then measure in quiescence.

Thermodynamic modeling was carried out by using the Gibbs free energy minimization program GEM-Selektor v3.7. The cement database Cemdata'18 [44] and PSI-GEMS thermodynamic database [45] were used to simulate the general aqueous, and gaseous species in the pore solution of C_3S with a gradient of pH values.

3. Results

3.1. Hydration of TC_3S with high solution to solid ratios

TC_3S with an empirical formula of Ca_3SiO_5 (Ca_2SiO_4·CaO) has a molar mass of 228.3 g/mol. a w/c of 100 needs to consume more than 1/6 of Ca (22.5/131.4 from Table 1) in the solid to achieve a saturation state (>22.5 mol/L [24,46]) with respect to portlandite at 25 °C. When the water/solid ratio is up to 200, it needs to consume more than 1/3 of solid C_3S to get this saturated condition. However, the heat flow in Fig. 2a shows that a high w/c only induces a higher hydration rate at the main peak, but it has no evident influence on the duration of the IP. Furthermore, the accumulative heat release in Fig. 2b shows that the heat release from the start of the IP to the main peak is similar among samples with the solution to C_3S ratio of 100, 200, and 200 (pH = 4). This value is about half of the heat release at 24 h. It implies that the dissolution degree of the solid is similar at the end of IP even with a rather high w/c, so the Ca concentration in the bulk pore solution from the high w/c is far from equilibrium during IP. 0.05 mmol/L H_2SO_4 solution (pH = 4) makes the main peak occur earlier, increases the heat release rate before 6 h, but has few effects on the ending time of the IP. An increase in the H_2SO_4 concentration up to 0.05 mol/L (pH = 1) alters the reaction of C_3S into one heat release peak without the IP. The high H^+ concentration in solution will bring a neutralization effect which results in a high heat release at the first peak, because the ionic O in C_3S undergoes a fast electrophilic attack from H^+ [21]. This also results in a different precipitation process, which will be further indicated by XRD.

Table 1
The ideal Ca^{2+} concentration from a complete dissolving of C_3S in a high water/solid ratio.

w/c (by weight)	Volume of water (mL)	Mole of Ca in solid (mmol)	The ideal Ca concentration (mmol/L)
100	100	13.14	131.4
200	200		95.7
600	600		21.9

Hydration products at 4 h were detected and presented in Fig. 3. It shows that gypsum is the main product of C_3S reacting with a high concentration H_2SO_4 (pH = 1). Most of the C_3S has reacted with sulfuric acid before 4 h. The dissolution of C_3S in H_2SO_4 solution (pH = 1) and precipitation of gypsum is a consecutive process without the occurrence of an IP. The w/c has little influences on the precipitation of CH at 4 h, which time is near the end of the IP. We can observe that the majority of solid residue is C_3S in good crystalline state even for a w/c of 600. A complete dissolution of C_3S with a w/c of 600 can only get 21.9 mmol/L Ca^{2+} in pore solution (Table 1), which is slightly lower than the saturation concentration (22.5 mmol/L) of portlandite. Moreover, the high diffraction intensity of C_3S indicates that its dissolution rate in such a high w/c is rather lower than the expected value referring to the dissolution theory. Apparently, the low Ca concentration in the solution (less than 21.9 mmol/L) implied an undersaturated state in the IP but it still resulted in the precipitation of CH (as shown in Fig. 3). This phenomenon can hardly be explained by the theory that the hydration rate is mainly controlled by dissolution rate with respect to the thermodynamic state of the bulk pore solution, as discussed in [47].

3.2. Hydration of TC_3S with KOH and K_2SO_4 solution

Many investigations focused on the dissolution of tricalcium/dicalcium silicate during the early hydration age based on a highly diluted solution [47–50]. These results could be well illustrated by the dissolution theories from geochemistry for silicates or other minerals [9,10,51], which are not coupled with the precipitation of new phases during dissolution. However, as mentioned in the previous section, the dissolution theory regarding the thermodynamic properties of the bulk solution is not so effective for explaining the hydration with a high w/c. This section will focus on the coupled nucleation and growth of hydration products during the IP.

Fig. 4 presents the hydration heat flow of TC_3S with deionized water, KH and KS, respectively. We define the IP as a time interval between the first and second peaks, during which the first derivative of the heat flow is between −0.5 mW/(g·h) and 0.5 mW/(g·h). The light was shed on the period from the starting point to the end of the IP. Comparing with 20 °C, a temperature of 25 °C brings an earlier starting point for samples with deionized water or KS. The IP starts at about 0.75 h after water addition except for KH (at about 0.5) at 25 °C, but this time is about 1 h for all samples at 20 °C. The IP ends up earlier in the hydration of samples at a higher temperature. This effect is so evident for samples with KH and KS, decreasing from 1.75 to 0.50 h and 2.28 to 1.15 h, respectively. K_2SO_4 has a great increasing effect on the main peak that is even larger than KOH, but the DIP is still longer than the sample with KOH. This is similar to the influence from sodium salts [27]. It may be related to the growth of products, which requires a focus on the early precipitated phases.

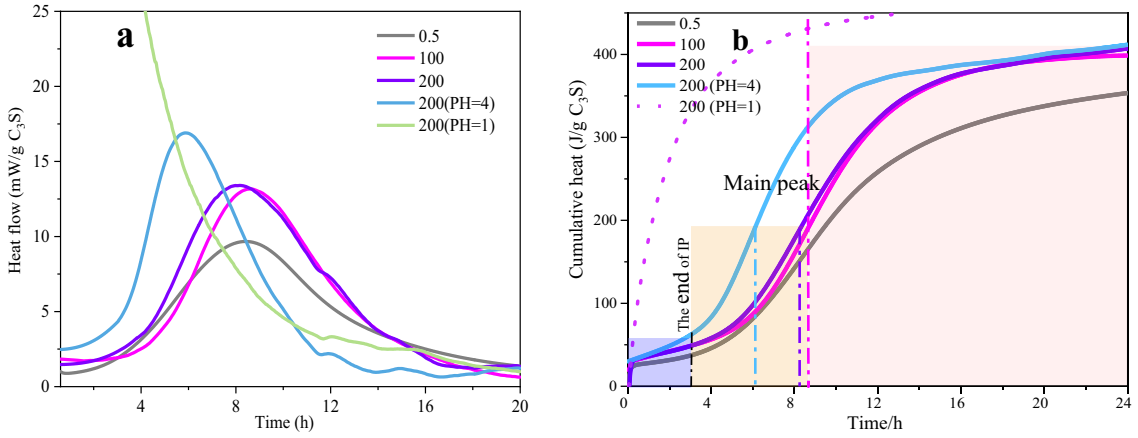

Fig. 2. Curves in "a" are the hydration heat flow of TC_3S with different w/c (0.5, 100, 200) and a sulfuric acid to C_3S ratio of 200 with two different pH values (pH = 4 and 1). Curves in "b" are the cumulative heat of samples with a w/c of 0.5, 100, 200 and a sulfuric acid to C_3S ratio of 200 (pH = 4 and 1).

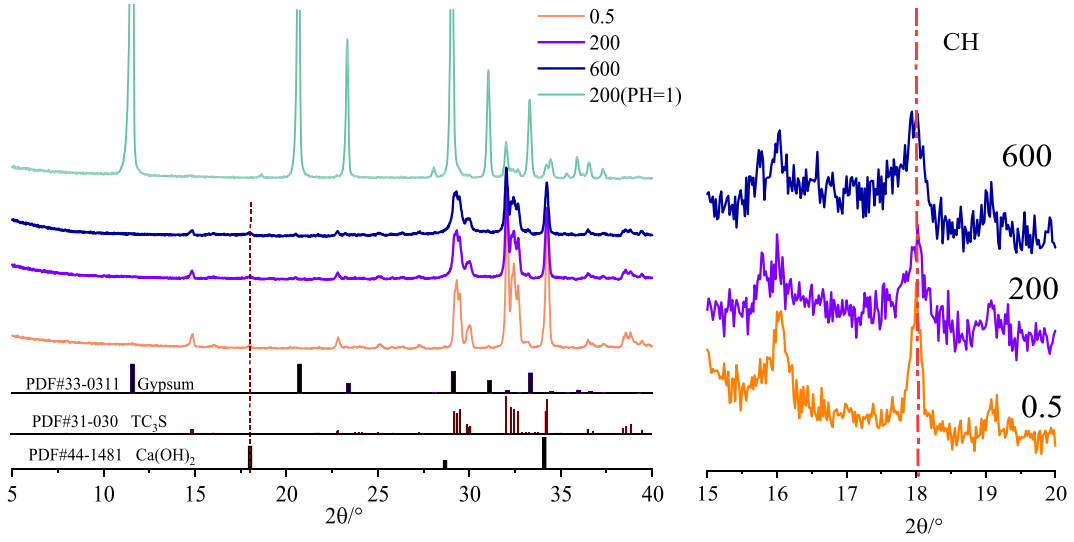

Fig. 3. XRD patterns of hydration products from samples with a w/c of 0.5, 200, and 600 and a sulfuric acid to TC_3S ratio of 200 (pH = 1). The hydration of sample was stopped at 4 h after water addition by isopropanol exchange.

Fig. 5 shows the surface of TC_3S hydrated in deionized water. It should be noted that the surface was treated with isopropanol, so it is different from the original hydrating surface. There is no distinguishable dissolution pit on the surface. However, we can observe many strips which were called needles in other published studies [27,52,53]. An enlarged image shows a clearer feature for the strips, and the strips consist of globule flocs. According to Jennings [54], these globule flocs with a size about 50 nm are from the packing of globules with a smaller size of 4–10 nm. From the Gaussian distribution of the measured values, it shows that the mean diameter of the globule flocs is about 63 nm.

The morphology of hydration products is more reasonable to be explained by a nonclassical nucleation theory. It is crystallization by particle attachment (CPA), which means a crystallization process by the addition of particles, ranging from multi-ion complexes to the fully formed nanocrystals [55]. In contrast, classical nucleation theory is crystallization through monomer by monomer addition [56]. As summarized in [55], particle attachment is influenced by the structure of the solvent and ions at solid-solution interfaces and in confined regions of the solution between solid surfaces. This nucleation process has been proven in the nucleation of many minerals, such as gypsum [57], iron oxyhydroxide nanoparticles [58], $CaCO_3$ [59], and silicates [60]. By applying this theory, we found that nucleation of C-S-H in the IP firstly comes with a formation of primary globule flocs (Fig. 5), which may be formed from polymerization of mono silicic complexes into dimeric structures [61]. This happens within a confined region between the surface and solution, because this region has a higher concentration of ions or complexes compared to the bulk solutions. From this point of view, the hydration in a highly diluted system is possible to have a precipitation of CH. Moreover, the dissolution equilibrium during the IP may build up within the interfacial regions instead of between the solid and bulk pore solution. Some correlations may exist between the thermodynamics of the interfacial region and bulk solution, but it is ambiguous to connect the hydration kinetic in the IP directly with the ion concentration in the bulk pore solution when the correlation is not clearly revealed.

The SEM images of the early hydration products from TC_3S with KH and KS are shown in Fig. 6. The strips on the surface of the sample in the KH (Fig. 6a) is much thinner than those precipitated in the deionized water (Fig. 5), and many strips even pack together to form a dense cluster. This is similar to the morphology of C-S-H precipitated from the hydration in sodium alkali solution [27,62]. Previous research paid attention to the needle length without considering the thickness of the needles that represents the diameters of the primary globule size. The mean thickness of the strips in KH is about 18 nm. Whereas the strips in

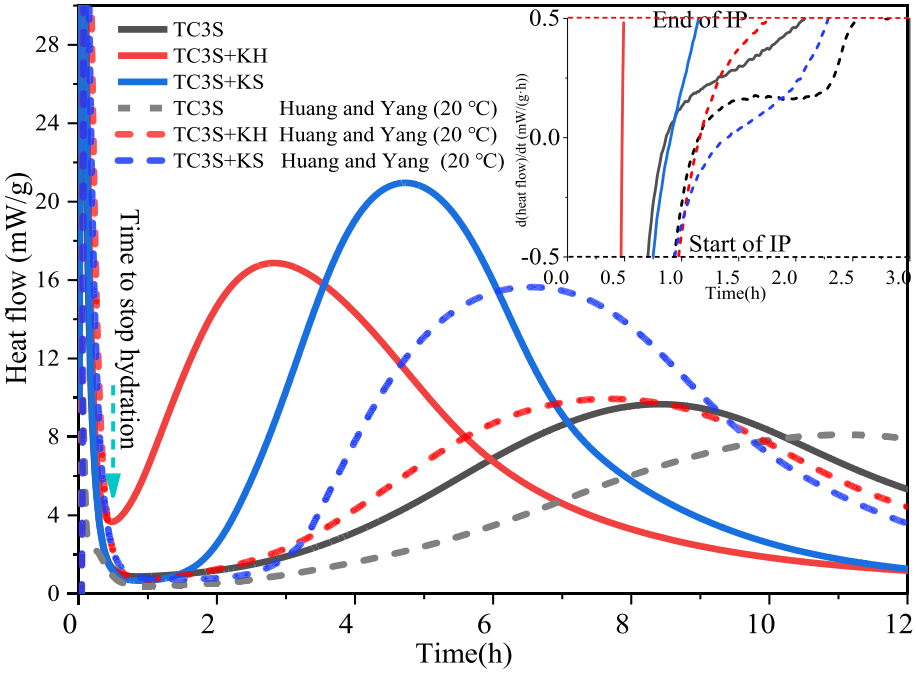

Fig. 4. Hydration heat flow of TC_3S with deionized water, KH and KS. The solid line is hydration data with a w/c = 0.5 at 25 °C, and the dash line is hydration data with a w/c = 2 at 20 °C, adopting from [29].

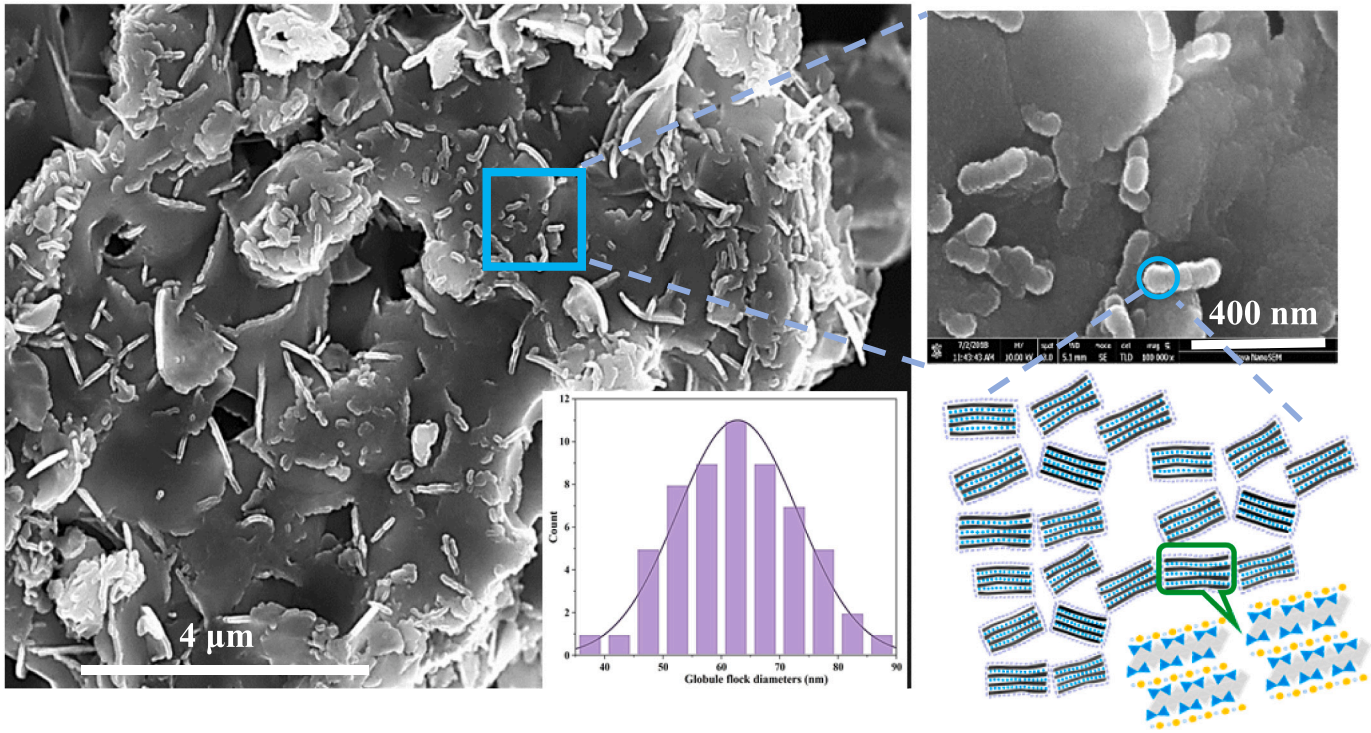

Fig. 5. SEM image of TC_3S hydrated with deionized water. The hydration was stopped at 0.5 h after water addition by isopropanol exchange. An enlarged image was provided to give a clearer picture of the particles on the surface. The diameter of the globule flocs was counted with the Nano measurer software. The structure of the globule flocs was illustrated based on Jennings model.

KS have a thickness about 49 nm, and this is much larger than the products precipitated in the KH. Furthermore, CH on the surface is well nucleated in large crystal, with some sizes larger than 500 nm. The correlations between the DIP (Fig. 4) and globule floc size will be further analyzed in the discussion section.

3.3. Hydration of TC_3S with C_3A

Fig. 7a shows the heat flow of TC_3S with C_3A, and Fig. 7b presents the comparison of the IP between hydration of TC_3S with and without C_3A. The presence of C_3A evidently prolongs the starting point of the IP. It increases this time to 2 h after water addition, which is much longer than

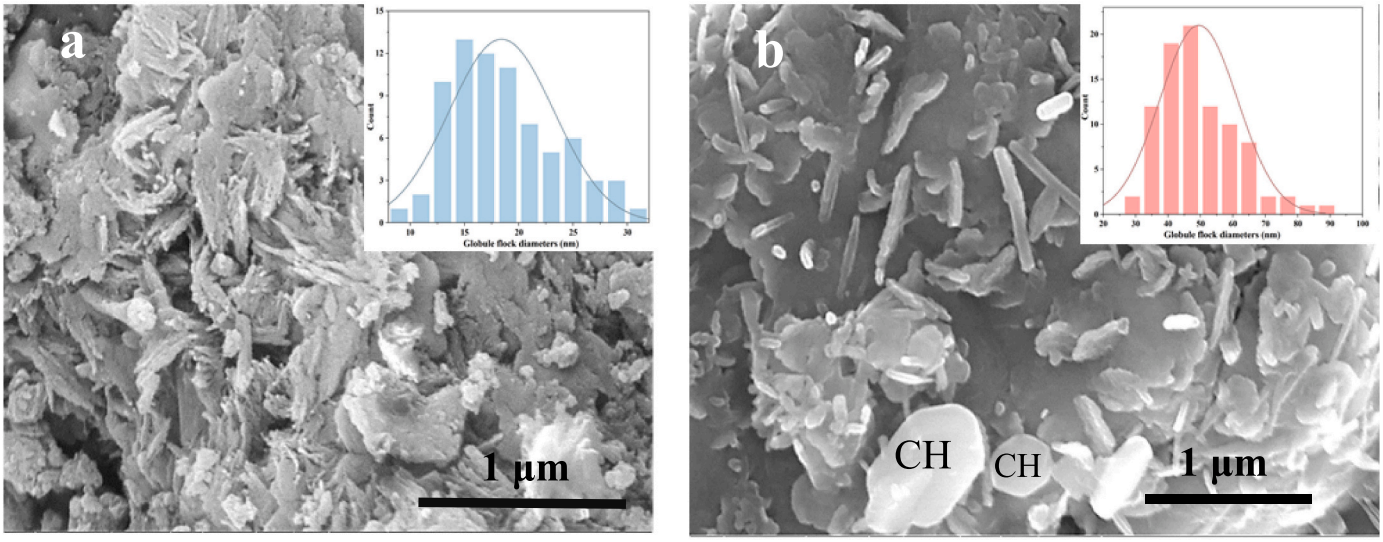

Fig. 6. SEM images of TC_3S hydrated in KOH (a) and K_2SO_4 (b) solutions, respectively. The hydration was stopped at 0.5 h after water addition by isopropanol exchange.

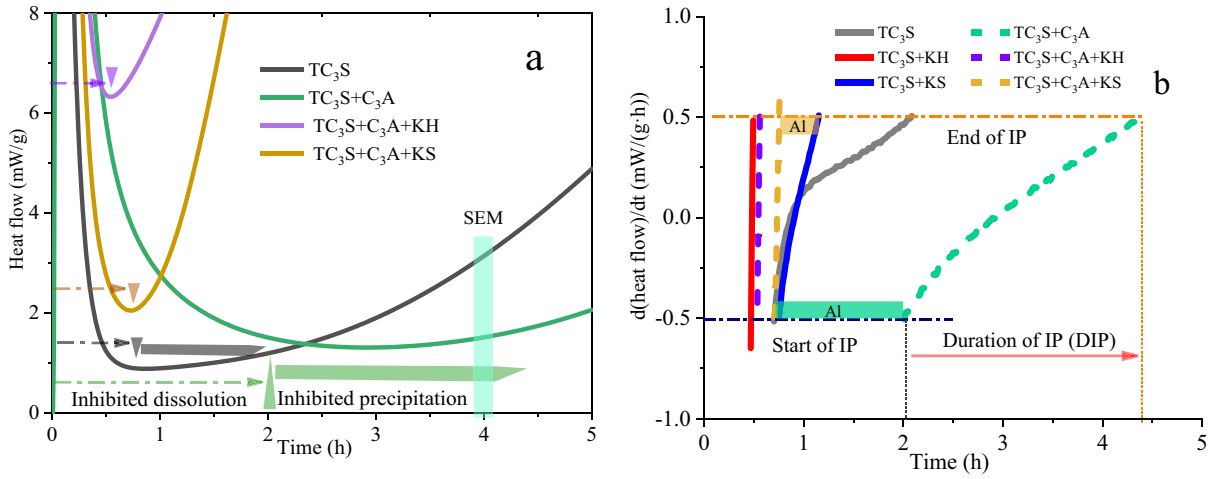

Fig. 7. Hydration heat flow of TC_3S with the presence of C_3A (a). The intervals of IP from TC_3S hydrating in solutions with and without C_3A (b). Samples were mixed with a w/c of 0.5 and cured at 25 °C.

the pure C_3S. A majority of the previous work hold the opinion that the prolonged IP came from inhibiting of C_3S dissolution [63,64], but the "Induction period" in their work was from water addition to the end of the low heat release rate period. Herein, we distinguish the inhibiting effect from aluminates on dissolution and nucleation. If we replace the concept of thermodynamic state between the solid and bulk solution with the state within the interfacial regions near the surface, according to [52], the sharp decrease in the heat release comes from an increase in saturation degree within the near surface with respect to C_3S dissolution. The delayed starting point of the IP (shown in Fig. 7b) is due to the inhibiting effect on dissolution by absorbing Al species on the surface of C_3S. In this period, the pH value is normally lower than 12.6. As hydration proceeds, the pH increases to a value larger than 13; this effect on dissolution will be eliminated [65,66]. As found in many published articles, the coverage effect of Al is negligible when pH is higher than 12.5 [67] and even at 10 for $Ca_{0.87}Al_{1.29}SiO_{4.81}$ [68]. When it comes to the start of IP, the pH of the pore solution in C_3S with C_3A is up to 12.5–13 [63], so the Al in solution have little effect on the dissolution of C_3S during this period. This is consistent with the result that the lowest heat release rate of C_3S with C_3A in IP is even higher than that of pure C_3S in IP (Fig. 7a). The ending time of the IP is delayed partially due to the inhibition of dissolution so the increment in DIP is shorter than the delayed starting time of the acceleration period, which is similar to the effect found in [69]. The increase in DIP by C_3A is much more effective in a previous article with a more reactive C_3A [63]. It comes from the inhibiting effect on both dissolution and nucleation.

KH and KS can eliminate the effect from C_3A on the IP and even shorten the DIP. The starting point of the IP from mixture system in KH is close to that of pure C_3S in KH because a high pH from KOH can avoid the suppression on the dissolution from Al ions. Moreover, the lowest heat release rate from the sample in KH is much higher than that of other samples (Figs. 4 and 7a). It implies that the dissolution rate of C_3S in KH is higher than that in other solutions when the nucleation of the hydration products takes over the hydration process. The K^+ and high pH in solution accelerate the nucleation, resulting in a reduction of the DIP. KS also can eliminate the effect from Al due to the reduction of the Al concentration by the precipitation of ettringite. Although C_3A has little influence on the starting point of C_3S in KS, it reduces the DIP. To reveal this, more attention should be paid to the nucleation and growth of the hydration products.

Fig. 8 presents the SEM images of TC_3S hydrated with deionized water. The hydration was stopped at 4 h by freeze-drying, which is

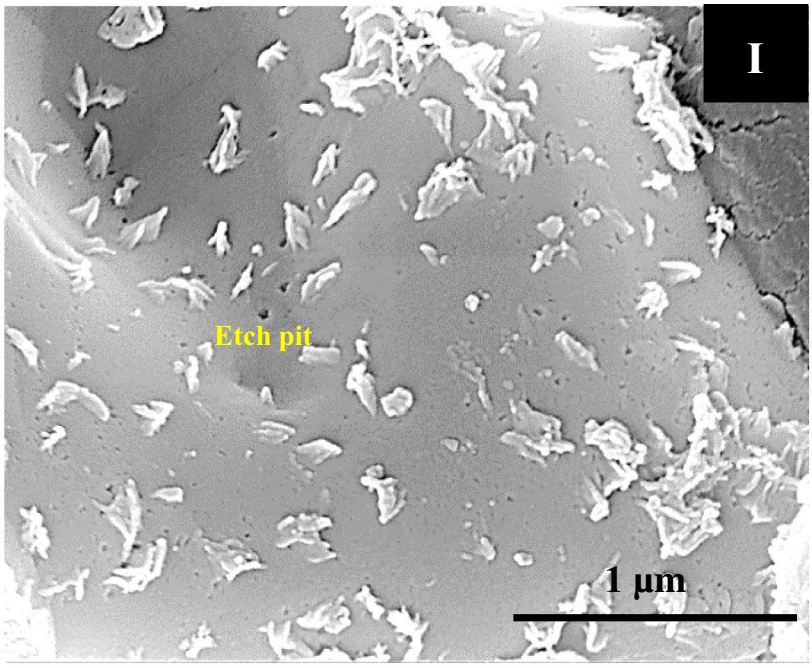

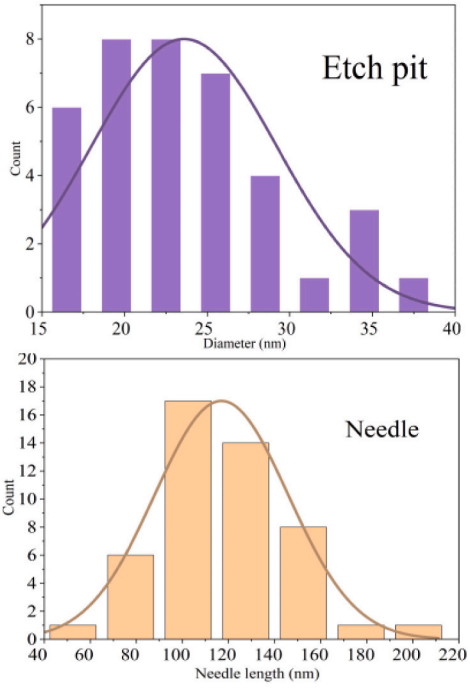

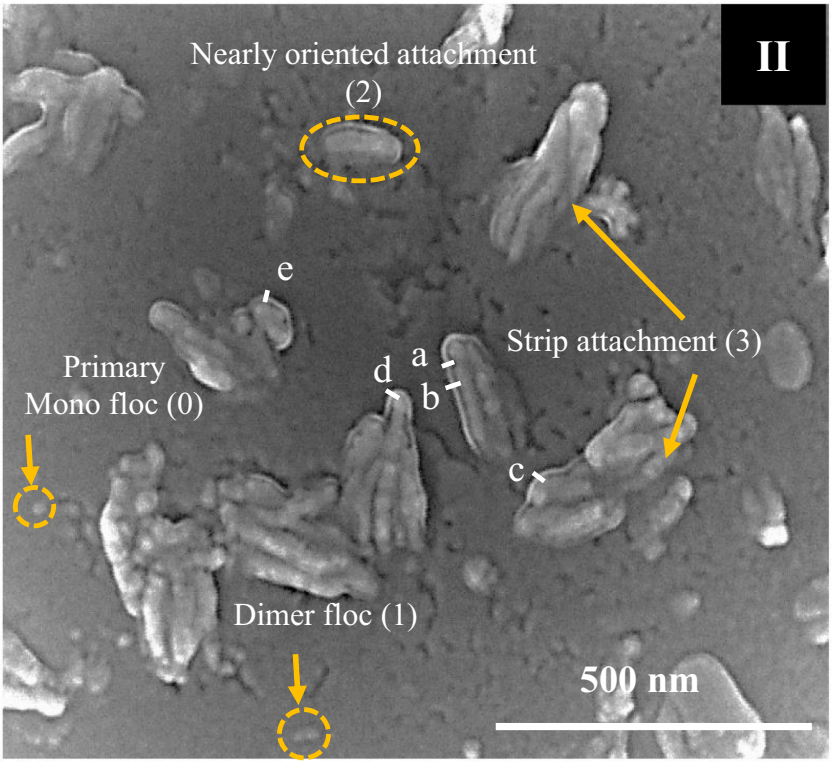

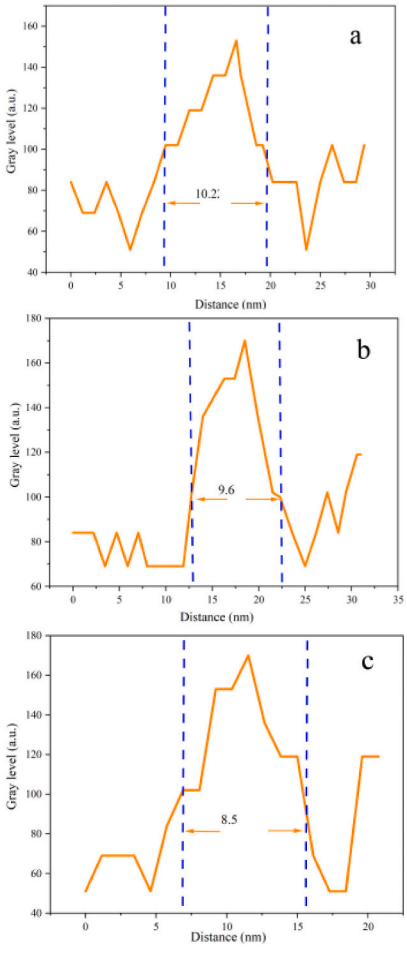

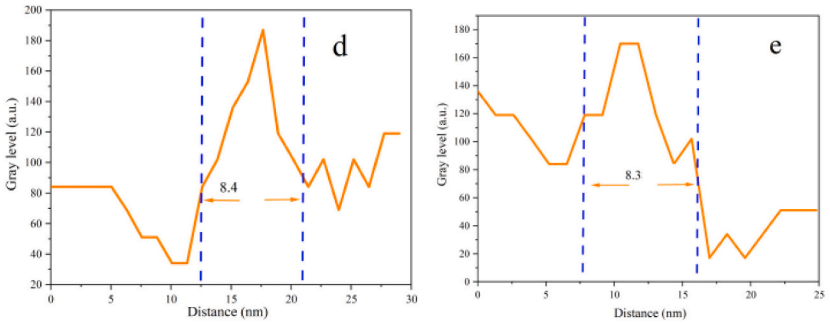

(caption on next page)

Fig. 8. SEM images of TC_3S hydrated in deionized water. The hydration was stopped at 4 h after water addition by freeze-drying. An image with a higher magnification was provided to give a clear picture of the particles on the surface (II). Nucleation of primary mono-flocs and dimer flocs were detected above or near the etch pit. C-S-H grows by nearly oriented attachment and block attachment. A layer of portlandite with a thickness of approximately 8–11 nm was detected between the undissolved surface and globule.

different from the treatment of samples in Fig. 5. The pristine feature of the surface is better preserved by freeze-drying than isopropanol exchange, as we can observe many etch pits on the surface of the particles. By counting 38 sites, the mean diameter (width) of the etch pits is about 24 nm. The length of C-S-H strips (clusters) is about 117 nm from counting 48 sites. The second image (Fig. 8II) with a higher magnification shows a clear feature of the particle surface. In the local region above the etch pits or near it, we can observe evidence for the nucleation of a primary mono floc (0), formation of a dimer floc (1), a single strip from the nearly oriented attachment (2) and the clusters from a strip attachment (3) or the single particle attaching to strips. This further proves that the precipitation of C-S-H starts from the nucleation of primary mono flocs that are poorly crystalline nanoparticles or colloidal, like the crystallization process of some other polymers or minerals [55,70]. The mono floc seems to be the intermediate C-S-H phase during the precipitation process as highlighted in the previous investigations [71,72]. Because it is thermodynamically metastable, it will aggregate into strips by the oriented attachment in a local region. With the increasing nucleation of mono floc and strips, the mono floc can also attach to the strip. Meanwhile, the strips may attach to each other to form a more stable cluster (block).

A linear gray level distribution in Fig. 8a-e indicates that a special layer exists between the precipitated C-S-H and undissolved surface. According to some experimental research on the dissolution of β-C_2S [73], there is an accumulation of Ca in the etch pit. This phenomenon may also occur in hydration of C_3S, so this layer would be portlandite that precipitates from the Ca ions absorbed on the colloidal surface in solution. A CH rim with a micron thickness was also detected between the hydration products and unhydrated mineral at 1 day [74]. In SEM images, the thickness of this layer is approximately 8–11 nm. Since the primary globule floc is the attachment of colloid [55,70], the double layer thickness of colloid may have some correlations with the precipitated layer. According to [75], the typical double-layer thickness of colloid at varying concentration can be estimated by:

$$\kappa^2 = \frac{F^2 \sum c_i z_i}{\varepsilon_r \varepsilon_0 RT} \tag{1}$$

where the reciprocal of κ is called the Debye length (namely, the double-layer thickness), F is Faraday's constant, R is the gas constant, T is the temperature in Kelvin, and ε_r and ε_0 are the relative permittivity and permittivity in a vacuum, respectively. c_i and z_i are the concentration and charge number of ions in solution, respectively. During early hydration of C_3S with deionized water, the main ions in the solution is Ca^{2+} and OH^- whose concentration is approximately 25 and 36 mmol/L respectively [76]. Under this molarity and with $\varepsilon_r = 78.5$ (water) at 298 K, we can get a value of 2.07 nm for Debye length. It is smaller than the thickness of the layer in Fig. 8II. Given that both the surface of dissolved C_3S and nucleated C-S-H are colloidal structure, the stable distance between these two colloids is about 8–14 nm under the condition when the colloids have a charged surface (10–100 mV) in a solution with ion concentration in range of 10–100 mmol/L [77]. Because we did not stir the paste after the initial mixing, the layer between the strip and unhydrated C_3S probably precipitates by a quick accumulation of Ca ions between two colloidal surfaces during a sudden freeze drying.

Fig. 9 presents the surface of C_3S hydrated at 4 h in the presence of C_3A. Etch pits were also detected on the surface (Fig. 9a1). The mean diameter of etch pits is about 28 nm, which is a little larger than that of pure C_3S in Fig. 8. Learning from the dissolution theory regarding the saturation state of bulk solution [78], the low reaction plateau (low heat release in Fig. 5a before 4 h) is controlled by the step retreat. However, the presence of etch pits in both Fig. 8 (pure C_3S) and Fig. 9a (C_3S with C_3A) indicates that this period is indeed controlled by the etch pit opening. In the IP, the transition happens from the step retreat to dislocation control (etch pit opening). To reveal the difference between the dissolution of C_3S with and without C_3A, we performed a further analysis based on the dissolution rate determining equation in [78].

$$|R_d| = \frac{A_1(1 - SI)|ln(SI)|}{1 + A_2|ln(SI)|} \tag{2}$$

$$SI = \frac{Q}{K_{SP}} \tag{3}$$

where A_1 and A_2 can be considered constants in this situation. R_d is the dissolution rate controlled by the etch pit opening. SI is the saturation index, Q is the ion product, and K_{sp} is the ion-product equilibrium constant. Based on Eq. (2), we can conclude that the dissolution rate of same C_3S particles with similar distribution of etch pit only relates to the saturation index of the solution. However, the previous articles [63,69] indicated that no significant difference was found between the main ions concentration in the pore solution of C_3S with and without C_3A under the IP. Hence, the big difference in heat flow at 4 h (Fig. 7a) can hardly be explained by rate controlling from the different dissolution rate of C_3S.

The nucleation and growth of the hydration products on the particle surface gives a reasonable explanation for the much lower heat release rate at 4 h. Fig. 9a2 shows that the needle length of C-S-H in the mixture system is about 94 nm, which is much shorter than this (116 nm) in pure C_3S. The diameters of the globule floc from C_3S with C_3A are even smaller than pure C_3S. Al ions in the solution induce the nucleation of the primary globule in a smaller size, but it suppresses the growth of strips from the attachment of primary particles. KH and KS can eliminate this inhibiting effect. The growth of C-S-H in KH and KS was much faster than it in deionized water, so the surface was covered by the hydration products as shown in Fig. 9b and c. The aluminates phase (stratinglite or ettringite) is hardly detected under SEM image. A comparison of the globule size in Fig. 9d shows that KH and KS can decease the globule floc size to about 20 nm. It is worth noting that the presence of C_3A almost erased the difference between the effect from KH and KS on the floc size, which is found in pure C_3S hydration (Fig. 6). With this observation, it is obvious that the long DIP from pure C_3S with KS (Fig. 6b) is due to the nucleation of larger primary globule compared to KH. C_3A can weaken the effect from KS on the nucleation of globules, so it reduces the DIP of mixture system compared to the pure C_3S in KS (Fig. 7b).

4. Discussion

4.1. Ion species in the pore solution with respect to pH

The hydration of C_3S is a complex reaction process during which the dissolution of C_3S involves the precipitation of C-S-H and CH. The difference between the hydration evolution shown in Figs. 2 and 3 indicates that the pH impacts the precipitated phase in the products. The pH will greatly affect the ion species of Ca [79] as well as Si [80] in the solution. Fig. 10 presents the ion species in the pore solution of pure C_3S. Ca^{2+} decreases as the pH increases from 8 to 13.5 (Fig. 10a). In the meantime, $CaOH^+$ shows a sharp increase of about five orders of magnitude. The increasing pH makes Ca^{2+} transform into $CaOH^+$, $Ca(H_3SiO_4)^+$, and $Ca(H_3SiO_4)OH$ when the value is lower than 10.3, but $Ca(H_3SiO_4)^+$ decreases dramatically after this critical value. The change in Si species in the solution is much more complex and the evolution of

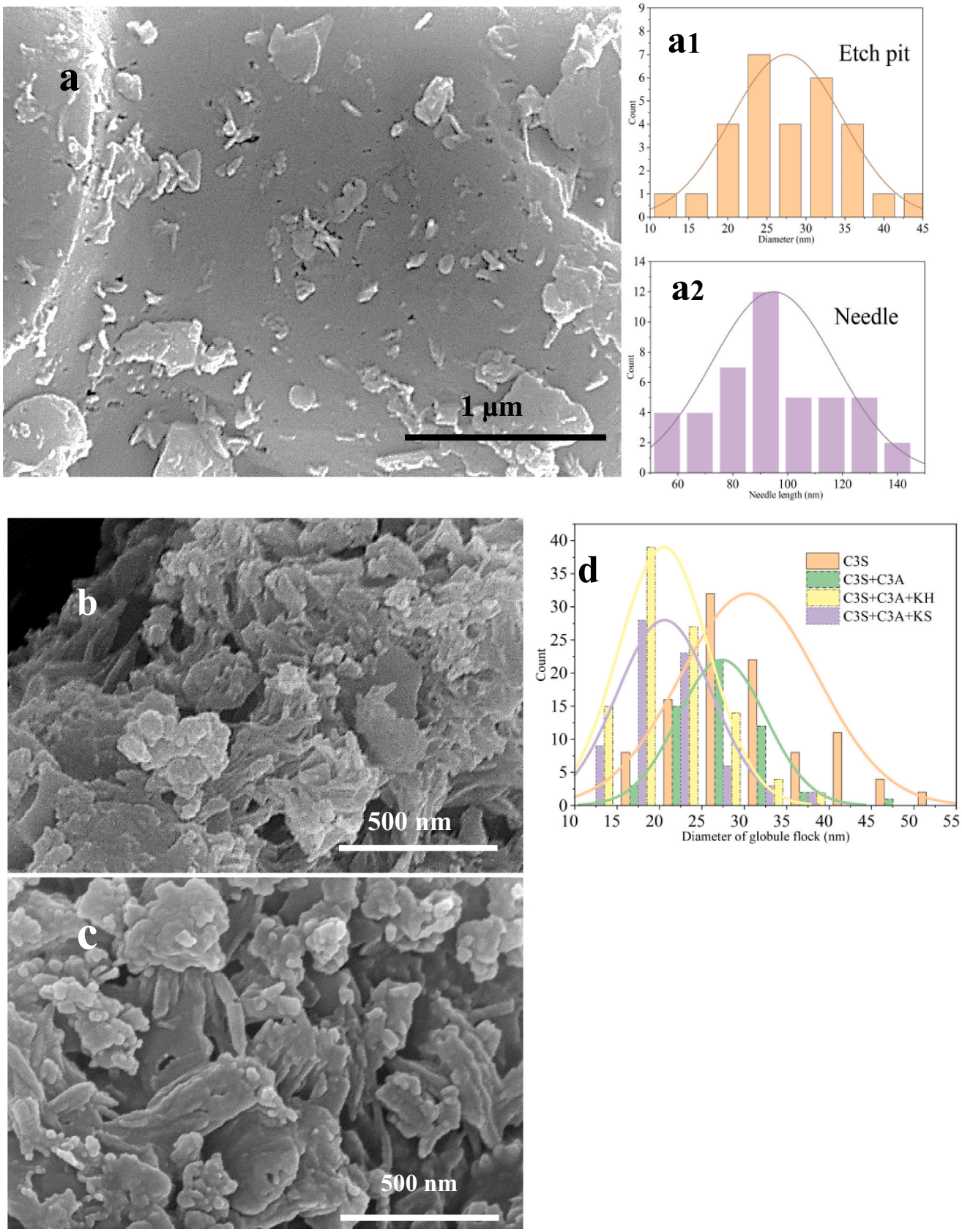

Fig. 9. SEM images of TC_3S hydrated with deionized water (a), KOH solution (b), and K_2SO_4 solution (c) in the presence of C_3A. The hydration was stopped at 4 h after water addition by freeze-drying. The diameter of the etch pit (a1) and needle length (a2) were counted for samples in deionized water. The diameter of the globule floc is summarized in d.

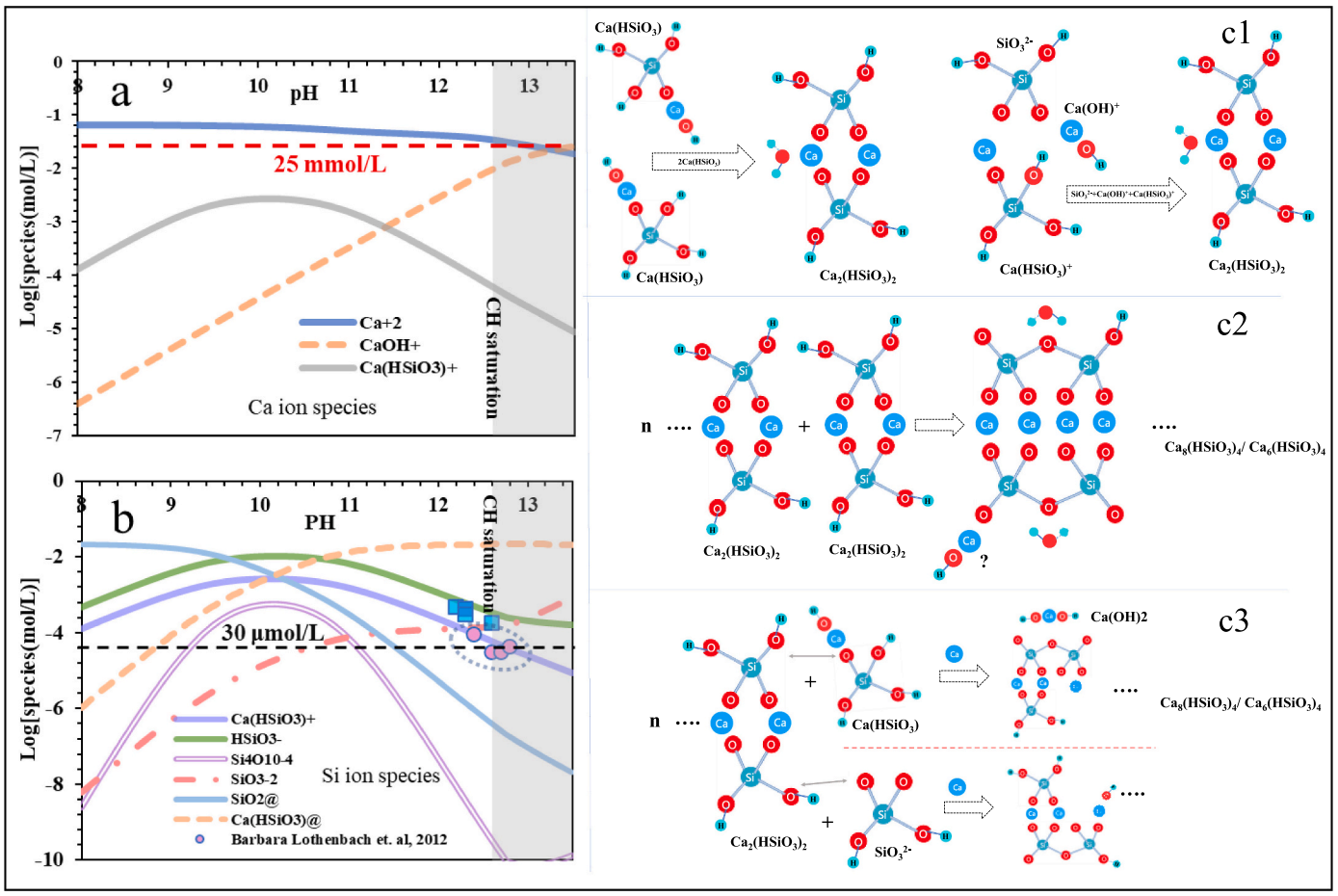

Fig. 10. Ca ion species (a) and Si ion species (b) in solution at different pH level from C_3S hydrated with deionized water (the results were simulated by GEMS, assuming it is without precipitation). The scatter data point is from reference [82] (the sphere is from the IP and the square is from the acceleration period). The c1 to c3 processes present the possible pathway to form the primary C-S-H structure.

some species in Fig. 10b is similar to the results in [80]. Because the pore solution of C_3S hydration is normally high alkaline (pH > 11), the thermodynamically stable species is comprised of $Ca(H_3SiO_4)OH$, $Ca(H_3SiO_4)^+$, $H_3SiO_4^-$, and $H_2SiO_4^{2-}$. The experimentally tested Si concentration in the pore solution during the IP is about 30 μmol/L at 25 °C [24,69,76]. As shown in Fig. 10b, the tested value is close to the concentration of $Ca(H_3SiO_4)^+$, and it decreases with the increase in pH. Many previous papers showed that the Si concentration has a decreasing trend as hydration proceeds before the end of the IP [24,69,76,81]. It may come from the decrease of $Ca(H_3SiO_4)^+$ caused by an increase of pH during this period. The spherical dot data from [82] fits well with the simulation results. The square scatters in Fig. 10a are data from the acceleration period, which may imply a different equilibrium state between the stable C-S-H and solution instead of the unhydrated C_3S surface and solution. If we focus on the reaction of C_3S at low pH, $SiO_2@(H_4SiO_4)$ dominates in the solution when the pH is lower than 8. According to [83], neither Ca^{2+} nor $CaOH^+$ can react with H_4SiO_4 from the thermodynamic aspect. Therefore, in the reaction of C_3S with H_2SO_4 (pH = 1), Ca ions will precipitate into $CaSO_4$ (see in Fig. 2) and the H_4SiO_4 species precipitate as amorphous SiO_2 [84].

As Taylor highlighted in [85], a preliminary Ca—O layer must be formed as a basis before the polymerization of SiO_4 into Si_2O_7. Fig. 10c1–3 illustrates the possible pathways for the formation of the primary C-S-H structure, and the reaction processes are summarized in Table 2. The possible polymerization process refers to the typical geopolymerisation of silicate [86]. The results from simulation based on density functional theory imply that the interaction between $CaOH^+$ and $H_2SiO_4^{2-}$ are the most favorable reaction in solution of pure C_3S [83].

Table 2
The possible reaction pathways for the C-S-H precipitation from the ionic complex in pure C_3S hydration.

Process	Reaction (use abbreviation from GEMS)	Bridge oxygen
c1	$2Ca(HSiO_3) \rightarrow Ca_2(HSiO_3)_2 + 2H_2O$ (left)	0
	$Ca(HSiO_3)^+ + SiO_3^{2-} + CaOH^+ \rightarrow Ca_2(HSiO_3)_2 + H_2O$ (right)	0
c2	(Preliminary complex structure) $Ca_{2n}(HSiO_3)_{2n} + Ca_2(HSiO_3)_2 \rightarrow Ca_{2n+2}(HSiO_3)_{2n}\text{-}Si_2O_5 + 2H_2O$	2
	$nCa_2(HSiO_3)_2 \rightarrow Ca_{2n}Si_{2n}O_{5n} + nH_2O$	n
c3	$Ca_{2n}(HSiO_3)_{2n} + Ca(HSiO_3) \rightarrow Ca_{2n}H_{2n-1}Si_{2n-1}O_{6n-4}\text{-}Si_2O_5 + Ca(OH)_2$	1
	$Ca_{2n}(HSiO_3)_{2n} + SiO_3^{2-} + Ca^{2+} \rightarrow Ca_{2n+1}H_{2n}Si_{2n-1}O_{6n-2}\text{-}Si_2O_5$	1

This is consistent with the thermodynamic simulation results by GEMS. Moreover, the interaction between Si species with $Al(OH)_4^-$ or Na^+ is highly possible as well, so the presence of these ions in solution will change the nucleation and growth of hydration products. Given that the c1 process is to build a good Ca—O layer basis for C-S-H, the $Ca(H_3SiO_4)OH$ species is critical for its nucleation and growth of it. As shown in Fig. 10b, a pH larger than 10.8 is a prerequisite to get enough $Ca(H_3SiO_4)OH$ species for a well-layered structure. This is consistent with XRD results from [87,88] in which C-S-H precipitated from pH less than 10.8 has few layer diffraction but the layer structure is evident for C-S-H precipitated from pH higher than that value. After a series of c1–3 reactions, the silanol exposed to the solution may deprotonate to form a

negative surface. As presented in [79], the $Ca(H_2O)_6^{2+}$ and $Ca(H_2O)_5(OH)^+$ will be absorbed on the negative silanol site for the next step reaction.

4.2. Hydration of C_3S up to the end of the IP

After C_3S is mixed with the solutions, the reaction of C_3S starts with a superficial dissolution and is followed by nucleation and growth of the products in local regions near the surface. The near surface thermodynamic state can be classified into 5 regimes as shown in Fig. 11.

4.2.1. Stage I: fast dissolution

This is the initial stage after minerals contact with water. This stage has a high superficial undersaturation state for the dissolution of C_3S, so it has an ultra-fast dissolution rate. It results in a high heat release peak in the calorimetry test (see Figs. 4 and 7 before 30 min). According to the transition state theory [89,90], since the initial stage is far from equilibrium, the dissolution rate is only correlated to two terms: the concentration of the activated complex and the frequency of these complexes cross the energy barrier. It can be expressed by Eq. (4) [91], where R_d denotes the dissolution rate, R^+ is the forward reaction rate, k stands for a rate constant and the concentration of the activated species is presented as [AB*]. AB* is the interfacial complexes exposed to the solution which include $>SiO^-$, $>SiOH_2^+$, >SiOH, and $>CaOH^+$ for C_3S due to the moisture in air [61]. Each complex has its own reaction rate constant, so the number of selective sites where the most active complex stay has a great impact on the initial dissolution rate of the minerals.

$$R_d = R^+ = k[AB^*] \tag{4}$$

It is obvious that ionic O and Ca have the quickest dissolution rate [66,92]. The dissolution starts with a hydrolysis of ionic O and Ca to form OH^-, Ca^{2+} in solution, and $CaOH^+$ attached on the surface (Fig. 11). Consequently, the pH and Ca^{2+} in the bulk solution increase evidently. Some ion species, like Al, in solution may absorb on the active sites to suppress the dissolution at a certain pH range (<12.5) [67]. Under this situation, the time to reach stage II and III will be delayed as shown in Fig. 7a.

4.2.2. Stage II: approaching dissolution equilibrium

As the quick initial dissolution proceeds, the increased pH and ion species in the solution augments the reverse reaction of the dissolution process. Under this condition, the thermodynamic state of the near surface region needs to be taken into account. Hence, the effective dissolution rate should be expressed by Eq. (5).

$$R_d = R^+\left(1 - e^{\frac{\Delta G}{RT}}\right) \tag{5}$$

where R^+ is the forward reaction rate in Eq. (4), ΔG is the Gibbs free energy difference between reactants and products, R represents the gas constant, and T is the absolute temperature. The local thermodynamic state may be close to the bulk solution when the liquid to solid ratio is as high as 10,000 or 50,000 [47]; thus, the dissolution rate has a good correlation with the thermodynamic state of the bulk solution. This is because such a high ratio induces the initial pH of the solution to be much lower than 11. $H_3SiO_4^-$, H_4SiO_4 and Ca^{2+} dominate the ion species in solution, and most of them will have good mobility into the bulk solution so it can be detected by ICP-OES. When it comes to the actual hydration with a low liquid to solid ratio (<10), the thermodynamic state of the bulk solution is different from the near surface region as we discussed in Section 3.1. Distribution of the ion species can also help to understand the argument about the congruency of dissolution during hydration. The Ca/Si in the pore solution depends on the liquid to solid ratio [93]. When pure C_3S or cement hydrates with a normal water/solid ratio, the typical Ca/Si ratio from the bulk pore solution during the IP is approximately 833 (25 mmol/30 μmol shown in Fig. 10), referring to the results from ICP-OES [24,23,69,76,82]. However, the Ca/Si ratio in the

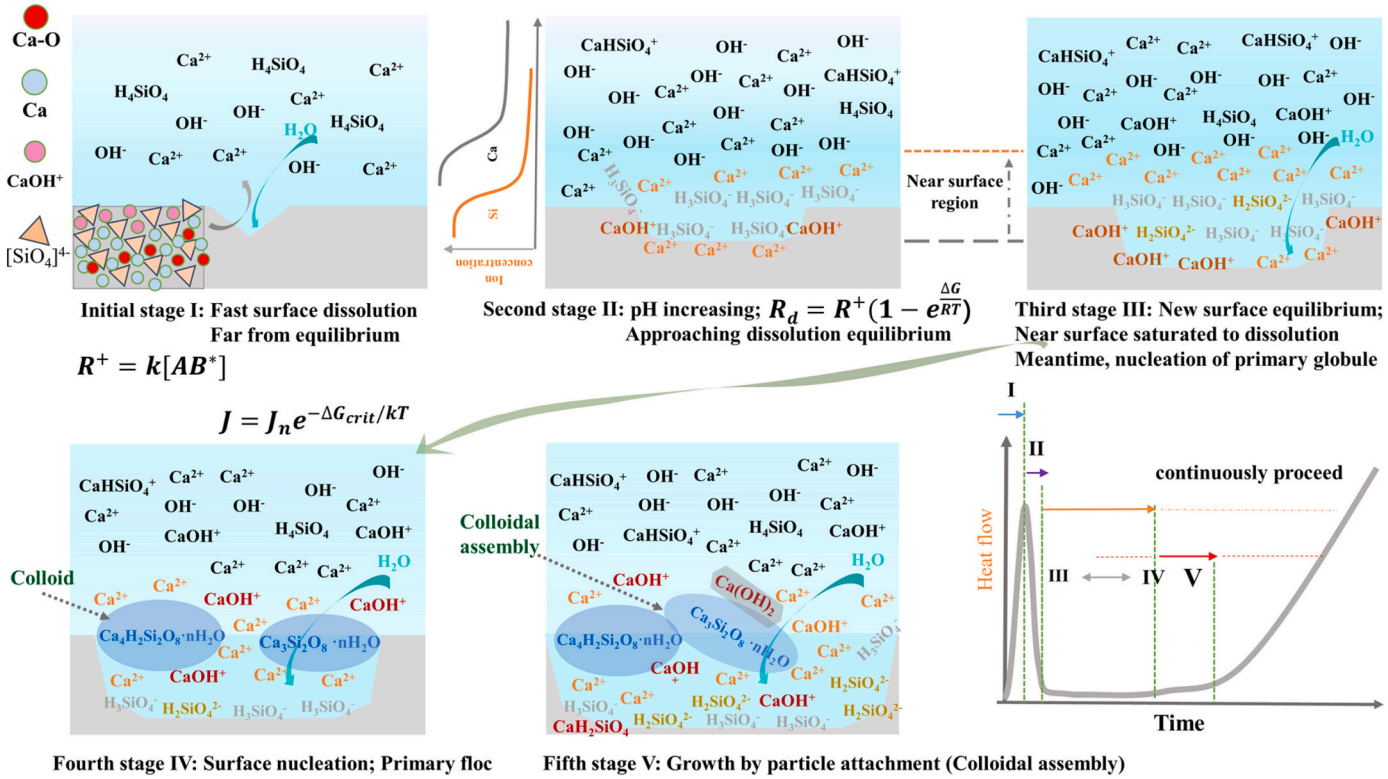

Fig. 11. Illustration of the hypothesis for hydration of C_3S up to the end of the low rate period. The ion species in black are ions far from the double layer with high mobility (that can be detected by filtering) and other colored notations of ions represent the surface absorbed species (hard to be detected in the pore solution). (For interpretation of the references to color in this figure legend, the reader is referred to the web version of this article.)

solution is close to 3 when water/solid ratio is very high [47]. This implies that the vast of number of Si ions on the surface can hardly move into the bulk solution whose pH is initially high due to the quick dissolution of ionic O and Ca in a limited content of water. Accumulation of $Ca(H_3SiO_4)OH$ on the selectively dissolved sites attracts cations (Ca^{2+} and $CaOH^+$) to form a cation layer. That is supported by the high positive zeta potential of hydrated C_3S and cement particles during the IP [94,95]. It may result in the formation of a locally concentrated region near the dissolution sites as shown in Fig. 11. The high local concentration of Si and Ca ions will build a near surface equilibrium with respect to dissolution even at a high water/solid ratio. Because it is a local equilibrium instead of a bulk equilibrium, the IP under a high w/c dissolution (100 or 200) will emerge at a similar time as under a normal w/c (0.5) (Fig. 2).

4.2.3. Stage III: new surface equilibrium

After a certain degree of dissolution, the near region comes to an equilibrium state with respect to dissolution of C_3S under static condition (without strong stirring). In the meantime, the high local concentration of Si and $CaOH^+$ ions will create an oversaturated state with respect to precipitation of primary C-S-H globules or CH. During the dissolution of minerals that is not involved with precipitation of new phases, it normally shows a low rate plateau in this period due to the step retreat [79]. Its low reaction plateau is controlled by the step retreat. However, the etch pit opening (see in Figs. 8 and 9) is the main dissolution process during the hydration of C_3S with the precipitation process in the IP (Fig. 7 at 4 h). The reaction rate in this period is controlled by the nucleation rate in the next stage instead of dissolution. Stage III and IV are two nearly concurrent stages during the hydration of TC_3S with water. However, the occurrence time of these two stages may be changed by the addition of admixtures.

4.2.4. Stage IV: surface nucleation

The primary C-S-H globules start to nucleate on the surface. The chemical structure of the globules could be with a Ca/Si ratio of 1.5, 2.0 [79], or even higher value because the deprotonation of silanol needs cations to neutralize the charge. The globule in solution will agglomerate into globule floc that is a colloidal structure as illustrated in Fig. 11 and shown in Figs. 8 and 9 in SEM image. The initial nucleation of the globule floc can be considered a classical nucleation process. The surface nucleation rate is given by [96–98]:

$$J = J_n e^{-\Delta G_{crit}/kT} \tag{6}$$

where J is the steady-state surface nucleation rate (number of nucleation events per surface area per second), ΔG_{crit} denotes the thermodynamic barrier to form a critically sized molecular cluster, and k represents the Boltzmann constant. J_n is a pre-exponential factor that can be considered a kinetic constant. The thermodynamic barrier is given with Eq. (7) by assuming a spherical nucleus:

$$\Delta G_{crit} = \frac{4\pi\gamma_{sl} r_{crit2}}{3} \tag{7}$$

where γ_{sl} denotes the surface energy and r_{crit} is the critical radius of the nuclei. A certain number of nuclei should be formed to achieve a high enough probability of attachment between the primary nuclei. During the hydration of C_3S we can assume that the required density of nuclei for C-S-H growth by attachment is n. The DIP of nucleation can be expressed as:

$$t_{ind} = \frac{n}{J} = \frac{n}{J_n} e^{\frac{\Delta G_{crit}}{kT}} \tag{8}$$

A combination of Eqs. (7) and (8) results in Eq. (9),

$$lnt_{ind} = ln\frac{n}{J_n} + \frac{\Delta G_{crit}}{kT} = A + \frac{4\pi\gamma_{sl} r_{crit2}}{3kT} \tag{9}$$

The DIP is from the end of stage II to IV. Fig. 12 shows a curve fitting between the duration of the induction period from hydration heat flow (Figs. 4 and 7) and the radius of globule flocs from SEM images (Figs. 5-6 and 8-9). The DIP has a good correlation with the globule size, especially in pure C_3S hydration stopped at 30 min with solvent exchange. The globule size of the hydration products stopped by freeze drying is much smaller than the products from solvent exchange, so the slope of the two fitted lines are significantly different. The triangle in Fig. 12 for pure C_3S deviates from the sample with C_3A, which implies the presence of Al will affect the kinetic of C-S-H nucleation.

4.2.5. Stage V: attachment to growth

This stage is dominated by growth of C-S-H through particle attachment, and the attachment of C-S-H is a colloidal assembly process similar to the other minerals [70]. The attachment happens on a selective orientation, so the morphology of C-S-H is strip like. It greatly consumes the Si and Ca ion species in the local region to reduce the near surface saturation state. Therefore, the dissolution of unreacted C_3S will have a sharp increase simultaneously. A growing number of attachment sites from pre-nucleated C-S-H increases the probability of later attachment, and this leads to an exponential increase in the hydration rate, resulting in an acceleration period.

The different stages may mix with each other during the hydration. The dashed line in Fig. 11 just represents the transition of the predominant reaction. For instance, the range with a red arrow noted with a "V" means that stage V dominates at this stage, but it is accompanied with all the other reactions happening at the same time.

4.3. Interpretation of factors affecting the DIP

The natural feature of raw materials has an impact on the DIP. C_3S with different particle sizes, polymorphisms and annealing treatments have the discrete density of defects on the surface. The defects have little effect on the time for the solution to reach a saturated state with respect to dissolution in the near surface zone. The doping may influence the dissolution rate at the initial water contacting, but the saturated state comes within a few minutes or even seconds after the C_3S contacts with water [47]. Afterwards the near surface layer will go into a new equilibrium condition with respect to precipitation of products, so the nucleation and growth of products take over the reaction process. Since the nucleation will preferentially start at the impurity site, the surface point defects or steps [99], these sites on the minerals surface accelerates the nucleation of primary flocks. These sites correspond to the etch pit or

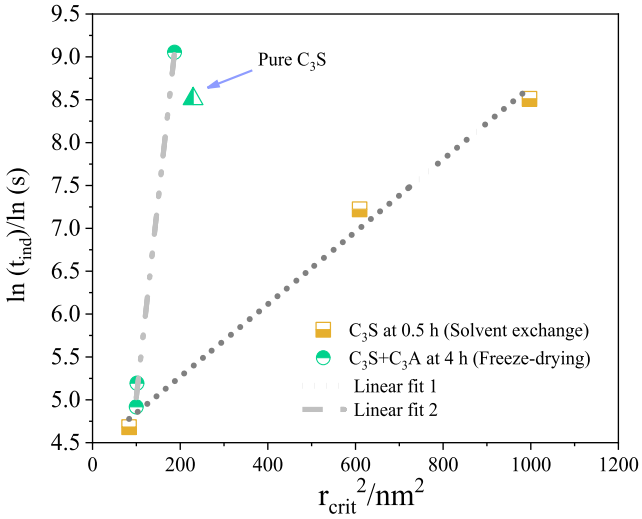

Fig. 12. The linear fitting data between ln (t_{ind}) and r_{crit}^2 based on Eq. (9).

region near it during hydration of C_3S (see nucleation site in Fig. 7). The slower dissolution rate also results in a lower number of nucleation sites thus reducing the nucleation rate of primary C-S-H. A lower etch pit density elevates the time for stage III and IV to reach a sufficient density of primary particles for further particle attachment.

The pH value is a critical parameter to control the DIP. A high pH (≥13) will facilitate the precipitation of C-S-H at a low Ca and Si concentrations, so the hydration may directly come into stage V from some point at stage II. C-S-H grows in a condition where the dissolution of C_3S is still at a relatively high rate, so the heat release at the inflection point is much higher than the control sample, as shown in Fig. 4. A sufficiently high alkalinity even eliminates the IP [36]. It implies that hydration starts from stage I and goes straight to stage V. Some soluble inorganic salts [32] or nano seeds [31,33,34] can shorten the duration of stage III and IV, because they have an enhancing effect on the nucleation of primary globule flocs. While some soluble inorganic salts ($CuCl_2$, $CuSO_4$, $Pb(NO_3)_2$) have an incremental effect on the DIP [17,26] because the metallic hydroxides from these salts will precipitate under a much lower pH than portlandite, these salts consume hydroxides and keep a relatively lower alkalinity in solution to slow down the nucleation of primary C-S-H (stage IV) and portlandite. Al ions have an inhibiting effect on the dissolution of C_3S, but this effect just shows in the first peak, corresponding to a delay in the transition from stage II to III, as shown in Fig. 7a. Al ions change the kinetic of nucleation of C-S-H primary globules as well. The longer DIP induced by Al ions is mainly due to its suppression on the growth of C-S-H.

Fig. 13 demonstrates that the Ca/Si ratio measured from the pore solutions is far from the stoichiometric ratio with 3 in solid. Some organics increase the solubility of C-S-H and it is so evident on the Ca^{2+} concentration. This makes the solubility of C-S-H closer to and even higher than the equilibrium line of C_3S hydration. Hexitols or some other organics enforce prolonging effects on the IP but increase the Si concentration in the bulk pore solution. The data dots for C_3S or white cement with retarding admixtures are higher than for the control sample, even being located on the upper part of the normal dissolution line (C_3S with C-S-H). The interaction between organic admixtures with Si ions will release more ions from the near region into the bulk solution, so the measured Si value was higher than the pure system. It modifies the double layer and will reduce the concentration of Si and Ca in the near surface region. This means that the precipitation of primary C-S-H on the surface with these admixtures requires a higher supersaturation state than in a solution without admixtures. When the dissolution of C_3S comes to stage II, the saturation state regarding precipitation in the near surface zone with the retarding organics is much lower than that in the plain system. Therefore, it has a lower nucleation rate at the end of stage II and requires a longer time to achieve a critical density of primary floc. Moreover, some organics will stabilize the primary flock, such as PCE [100]. It will hinder the attachment between primary particles, and consequently, the transition from stage IV to V will be prolonged.

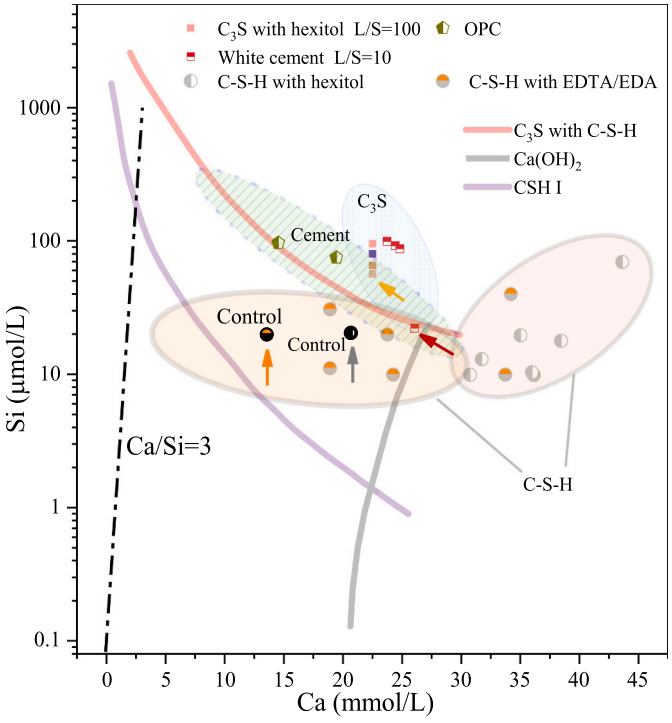

Fig. 13. Concentrations of silicon and calcium ions from the pore solution. The equilibrium lines of C_3S with C-S-H, CSH I and $Ca(OH)_2$ are adopted from [101]. Scatter data are from the pore solution of Portland cement during the IP [102], solution of C_3S [43]/white cement [38] with hexitols and C-S-H with the addition of organics [103]. Arrows point at the data dots from the control samples in the corresponding literature.

4.4. Limitations and perspective for further investigation

The dissolving surface and precipitated products are analyzed based on the SEM images of the treated samples instead of in-situ measurement. Therefore, the hypothesis is proposed based on the assumptions: Firstly, the solvent exchange treatment by isopropanol has the same effect on the precipitated products of samples hydrating in different solutions; Secondly, the freeze-dry method preserves the pristine feature of the particles surface and the plating of Au has few effects on the sizes and number of etch pit.

The chemical composition of the layer structure between C-S-H and the unhdyrated surface (Fig. 8) needs some direct evidence from the advanced equipment (such as HR-TEM [57]) with high resolution. The previous papers [69,76] concluded that the bulk pore solution reached an oversaturated state regarding the C-S-H during IP, so it implied a potential nucleation in the bulk solution. Although the nucleation on the surface defects or steps may be preferential, how does the homogeneous nucleation in pore solution contribute to the hydration process is lack of consideration in this hypothesis. It is better to include the homogenous nucleation model from [104] in the further investigation to complete the theory. The evidence for the nucleation of primary globules can hardly be detected under the SEM images, which may be due to the resolution limitations or the metastable state of it. According to the models from [54,104,105], the size of globule is about 3–4 nm, but we can only observe globule floc whose size is larger than 20 nm under SEM. We assumed that "n" is the sufficient density for the attachment of flocs to take over the hydration process. The investigation on determining this value is critical to prove this hypothesis.

5. Conclusions

The hydration of C_3S with a very high w/c is difficult to be explained by the dissolution theory with only with focus on the thermodynamic state of the bulk pore solution, because the dissolved percentage of C_3S detected from calorimetry and XRD test presents little differences between low (0.5) and high (200, 600) w/c. Therefore, more attentions should be paid to the nucleation of hydration products within the interfacial zone of the solid and solution.

From SEM images, the dissolution etch pit can be observed on the surface of C_3S particles whose hydration was stopped by free-drying near the end of IP. Al almost has no influence on the size of etch pit on C_3S at the end of IP. C-S-H precipitates on the etch pit or in region close to it. A nonclassical nucleation theory is better to explain the precipitation process of C-S-H during IP. It starts with nucleation of primary particles and then is followed by the growth from particle attachment. The attachment of C-S-H globule floc is a colloidal assembly process. A layer between the C-S-H floc and C_3S surface was detected, which probably is the precipitation of CH between the two colloidal

surfaces.

The increase in the heat release rate at the end of IP comes from the accelerating growth rate of C-S-H instead of dissolution of the etch pit. KOH and K_2SO_4 have an impact on the primary globule size and growth of strip C-S-H so that they change the DIP. Al ion inhibits the dissolution of C_3S at a very early age before the start of IP, and it also suppresses the growth of C-S-H to increase the DIP. The pH affects the Si and Ca ion species in the pore solution, which impacts both the dissolution of C_3S and the nucleation of primary particles.

Based on the dissolution and CPA theory, we suggest five stages in the early hydration process by focusing on the nucleation and growth of C-S-H within the local region, that is, Stage I: Fast dissolution, Stage II: Approaching dissolution equilibrium, Stage III: New surface equilibrium, Stage IV: Surface nucleation, and Stage V: Attachment to growth.

CRediT authorship contribution statement

Liming Huang: Conceptualization, Methodology, Software, Investigation, Data analysis, Writing-Original Draft, Writing-Review & Editing. Luping Tang: Writing-Review & Editing, Supervision, Project administration, Funding acquisition. Haitao Gu: Investigation, Resources. Zhen Li: Investigation, Resources. Zhenghong Yang: Review & Editing, Supervision, Project administration.

Declaration of competing interest

We declare no conflicts of interest.

Acknowledgements

The authors appreciate the financial support from the National Key Research and Development Program of China (No. 2018YFD1101002), and National Project of Sweden Formas (No. 20221012).

References

[1] J. Bensted, Hydration of Portland cement, in: Adv. Cem. Technol, Elsevier, 1983, pp. 307–347, https://doi.org/10.1016/B978-0-08-028670-9.50015-6.
[2] K. Scrivener, Advances in understanding cement hydration mechanisms, Cem. Concr. Res. 16 (2019).
[3] H.M. Jennings, P.L. Pratt, An experimental argument for the existence of a protective membrane surrounding Portland cement during the induction period, Cem. Concr. Res. 9 (1979) 501–506, https://doi.org/10.1016/0008-8846(79)90048-6.
[4] P. Juilland, L. Nicoleau, R.S. Arvidson, E. Gallucci, Advances in dissolution understanding and their implications for cement hydration, RILEM Tech. Lett. 2 (2017) 90–98, https://doi.org/10.21809/rilemtechlett.2017.47.
[5] M. Costoya, Effect of Particle Size on the Hydration Kinetics And Microstructural Development of Tricalcium Silicate, Ecole Polytechnique Fédérale de Lausanne (EPFL), 2008 (Doctoral Dissertation).
[6] I. Odler, J. Schüppstuhl, Early hydration of tricalcium silicate III. Control of the induction period, Cem. Concr. Res. 11 (1981) 765–774, https://doi.org/10.1016/0008-8846(81)90035-1.
[7] J.M. Makar, G.W. Chan, K.Y. Esseghaier, A peak in the hydration reaction at the end of the cement induction period, J. Mater. Sci. 42 (2007) 1388–1392, https://doi.org/10.1007/s10853-006-1427-3.
[8] J.W. Bullard, H.M. Jennings, R.A. Livingston, A. Nonat, G.W. Scherer, J. S. Schweitzer, K.L. Scrivener, J.J. Thomas, Mechanisms of cement hydration, Cem. Concr. Res. 41 (2011) 1208–1223, https://doi.org/10.1016/j.cemconres.2010.09.011.
[9] J. Schott, S. Brantley, D. Crerar, C. Guy, M. Borcsik, C. Willaime, Dissolution kinetics of strained calcite, Geochim. Cosmochim. Acta 53 (1989) 373–382, https://doi.org/10.1016/0016-7037(89)90389-X.
[10] R.T. Cygan, W.H. Casey, M.B. Boslough, H.R. Westrich, M.J. Carr, G.R. Holdren, Dissolution kinetics of experimentally shocked silicate minerals, Chem. Geol. 78 (1989) 229–244, https://doi.org/10.1016/0009-2541(89)90060-0.
[11] F. Bellmann, T. Sowoidnich, B. Möser, Formation of an intermediate phase and influence of crystallographic defects on dissolution of C3S, in: Proc. XIII Int. Congr. Chem. Cem, 2011. Madr. Spain.
[12] H.F. Taylor, Cement Chemistry, Thomas Telford London, 1997.
[13] L. Huang, W. Song, H. Li, H. Zhang, Z. Yang, Effects of aphthitalite on the formation of clinker minerals and hydration properties, Constr. Build. Mater. 183 (2018) 275–282, https://doi.org/10.1016/j.conbuildmat.2018.06.082.
[14] H.R. Stewart, J.E. Bailey, Microstructural studies of the hydration products of three tricalcium silicate polymorphs, J. Mater. Sci. 18 (1983) 3686–3694, https://doi.org/10.1007/BF00540741.
[15] D. Stephan, H. Maleki, D. Knöfel, B. Eber, R. Härdtl, Influence of Cr, Ni, and Zn on the properties of pure clinker phases part I. C3S, Cem. Concr. Res. (1999) 8.
[16] X.-W. Ma, H.-X. Chen, P.-M. Wang, Effect of CuO on the formation of clinker minerals and the hydration properties, Cem. Concr. Res. 40 (2010) 1681–1687, https://doi.org/10.1016/j.cemconres.2010.08.009.
[17] N. Gineys, G. Aouad, D. Damidot, Managing trace elements in Portland cement – part I: interactions between cement paste and heavy metals added during mixing as soluble salts, Cem. Concr. Compos. 32 (2010) 563–570, https://doi.org/10.1016/j.cemconcomp.2010.06.002.
[18] D. Stephan, S. Wistuba, Crystal structure refinement and hydration behaviour of 3CaO·SiO2 solid solutions with MgO, Al2O3 and Fe2O3, J. Eur. Ceram. Soc. 26 (2006) 141–148, https://doi.org/10.1016/j.jeurceramsoc.2004.10.031.
[19] D. Stephan, S.N. Dikoundou, G. Raudaschl-Sieber, Hydration characteristics and hydration products of tricalcium silicate doped with a combination of MgO, Al2O3 and Fe2O3, Thermochim. Acta 472 (2008) 64–73, https://doi.org/10.1016/j.tca.2008.03.013.
[20] A. Bazzoni, S. Ma, Q. Wang, X. Shen, M. Cantoni, K.L. Scrivener, The effect of magnesium and zinc ions on the hydration kinetics of C 3 S, J. Am. Ceram. Soc. 97 (2014) 3684–3693, https://doi.org/10.1111/jace.13156.
[21] E. Durgun, H. Manzano, R.J.M. Pellenq, J.C. Grossman, Understanding and controlling the reactivity of the calcium silicate phases from first principles, Chem. Mater. 24 (2012) 1262–1267, https://doi.org/10.1021/cm203127m.
[22] D.M. Kirby, J.J. Biernacki, The effect of water-to-cement ratio on the hydration kinetics of tricalcium silicate cements: testing the two-step hydration hypothesis, Cem. Concr. Res. 42 (2012) 1147–1156, https://doi.org/10.1016/j.cemconres.2012.05.009.
[23] C. Naber, F. Bellmann, J. Neubauer, Influence of w/s ratio on alite dissolution and C-S-H precipitation rates during hydration, Cem. Concr. Res. 134 (2020), 106087, https://doi.org/10.1016/j.cemconres.2020.106087.
[24] P.W. Brown, E. Franz, G. Frohnsdorff, H.F.W. Taylor, Analyses of the aqueous phase during early C3S hydration, Cem. Concr. Res. 14 (1984) 257–262, https://doi.org/10.1016/0008-8846(84)90112-1.
[25] P.W. Brown, C.L. Harner, E.J. Prosen, The effect of inorganic salts on tricalcium silicate hydration, Cem. Concr. Res. 16 (1986) 17–22, https://doi.org/10.1016/0008-8846(86)90063-3.
[26] S. Etris, Y. Fiorini, K. Lieb, I. Moore, A. Batik, D. Kantro, Tricalcium silicate hydration in the presence of various salts, J. Test. Eval. 3 (1975) 312, https://doi.org/10.1520/JTE10661J.
[27] B. Mota, T. Matschei, K. Scrivener, The influence of sodium salts and gypsum on alite hydration, Cem. Concr. Res. 75 (2015) 53–65, https://doi.org/10.1016/j.cemconres.2015.04.015.
[28] B. Mota, T. Matschei, K. Scrivener, Impact of NaOH and Na2SO4 on the kinetics and microstructural development of white cement hydration, Cem. Concr. Res. 108 (2018) 172–185, https://doi.org/10.1016/j.cemconres.2018.03.017.
[29] L. Huang, Z. Yang, Early hydration of tricalcium silicate with potassium hydroxide and sulfate from pore solution and solid view, Constr. Build. Mater. 230 (2020), 116988, https://doi.org/10.1016/j.conbuildmat.2019.116988.
[30] O. Mendoza, C. Giraldo, S.S. Camargo, J.I. Tobón, Structural and nano-mechanical properties of calcium silicate hydrate (C-S-H) formed from alite hydration in the presence of sodium and potassium hydroxide, Cem. Concr. Res. 74 (2015) 88–94, https://doi.org/10.1016/j.cemconres.2015.04.006.
[31] J.J. Thomas, H.M. Jennings, J.J. Chen, Influence of nucleation seeding on the hydration mechanisms of tricalcium silicate and cement, J. Phys. Chem. C 113 (2009) 4327–4334, https://doi.org/10.1021/jp809811w.
[32] F. Bellmann, Basic mechanisms of afwillite seeding for acceleration of tricalcium silicate hydration, Cem. Concr. Res. 132 (2020), 106030.
[33] T. Sato, F. Diallo, Seeding effect of nano-CaCO3 on the hydration of tricalcium silicate, Transp. Res. Rec. 1 (2010) 61–67, https://doi.org/10.3141/2141-11.
[34] B.Y. Lee, K.E. Kurtis, Influence of TiO2 nanoparticles on early C3S hydration, J. Am. Ceram. Soc. 93 (2010) 3399–3405, https://doi.org/10.1111/j.1551-2916.2010.03868.x.
[35] J.F. Young, A review of the mechanisms of set-retardation in Portland cement pastes containing organic admixtures, Cem. Concr. Res. 2 (1972) 415–433, https://doi.org/10.1016/0008-8846(72)90057-9.
[36] N.B. Milestone, Hydration of tricalcium silicate in the presence of lignosulfonates, glucose, and sodium gluconate, J. Am. Ceram. Soc. 62 (1979) 321–324, https://doi.org/10.1111/j.1151-2916.1979.tb19068.x.
[37] J. Pourchez, P. Grosseau, B. Ruot, Changes in C3S hydration in the presence of cellulose ethers, Cem. Concr. Res. 40 (2010) 179–188, https://doi.org/10.1016/j.cemconres.2009.10.008.
[38] C. Nalet, A. Nonat, Retarding effectiveness of hexitols on the hydration of the silicate phases of cement: interaction with the aluminate and sulfate phases, Cem. Concr. Res. 90 (2016) 137–143, https://doi.org/10.1016/j.cemconres.2016.09.018.
[39] R. Cook, H. Ma, A. Kumar, Mechanism of tricalcium silicate hydration in the presence of polycarboxylate polymers, SN Appl. Sci. 1 (2019) 145, https://doi.org/10.1007/s42452-018-0153-1.
[40] D. Marchon, P. Juilland, E. Gallucci, L. Frunz, R.J. Flatt, Molecular and submolecular scale effects of comb-copolymers on tri-calcium silicate reactivity: toward molecular design, J. Am. Ceram. Soc. 100 (2017) 817–841, https://doi.org/10.1111/jace.14695.

[41] J.W. Bullard, R.J. Flatt, New insights into the effect of calcium hydroxide precipitation on the kinetics of tricalcium silicate hydration, J. Am. Ceram. Soc. 93 (2010) 1894–1903, https://doi.org/10.1111/j.1551-2916.2010.03656.x.

[42] X. Kong, S. Emmerling, J. Pakusch, M. Rueckel, J. Nieberle, Retardation effect of styrene-acrylate copolymer latexes on cement hydration, Cem. Concr. Res. 75 (2015) 23–41, https://doi.org/10.1016/j.cemconres.2015.04.014.

[43] C. Nalet, A. Nonat, Effects of hexitols on the hydration of tricalcium silicate, Cem. Concr. Res. 91 (2017) 87–96, https://doi.org/10.1016/j.cemconres.2016.11.004.

[44] B. Lothenbach, D.A. Kulik, T. Matschei, M. Balonis, L. Baquerizo, B. Dilnesa, G. D. Miron, R.J. Myers, Cemdata18: a chemical thermodynamic database for hydrated Portland cements and alkali-activated materials, Cem. Concr. Res. 115 (2019) 472–506, https://doi.org/10.1016/j.cemconres.2018.04.018.

[45] T. Thoenen, W. Hummel, U. Berner, E. Curti, The PSI/Nagra Chemical Thermodynamic Database 12/07, 2014.

[46] E.M. Gartner, F.J. Tang, S.J. Weiss, Saturation factors for calcium hydroxide and calcium sulfates in fresh Portland cement pastes, J. Am. Ceram. Soc. 68 (1985) 667–673, https://doi.org/10.1111/j.1151-2916.1985.tb10122.x.

[47] L. Nicoleau, A. Nonat, D. Perrey, The di- and tricalcium silicate dissolutions, Cem. Concr. Res. 47 (2013) 14–30, https://doi.org/10.1016/j.cemconres.2013.01.017.

[48] P. Juilland, E. Gallucci, R. Flatt, K. Scrivener, Dissolution theory applied to the induction period in alite hydration, Cem. Concr. Res. 40 (2010) 831–844, https://doi.org/10.1016/j.cemconres.2010.01.012.

[49] L. Nicoleau, E. Schreiner, A. Nonat, Ion-specific effects influencing the dissolution of tricalcium silicate, Cem. Concr. Res. 59 (2014) 118–138, https://doi.org/10.1016/j.cemconres.2014.02.006.

[50] F. Bellmann, T. Sowoidnich, H.-M. Ludwig, D. Damidot, Dissolution rates during the early hydration of tricalcium silicate, Cem. Concr. Res. 72 (2015) 108–116, https://doi.org/10.1016/j.cemconres.2015.02.002.

[51] A.C. Lasaga, Variation of crystal dissolution rate based on a dissolution stepwave model, Science 291 (2001) 2400–2404, https://doi.org/10.1126/science.1058173.

[52] A. Ouzia, K. Scrivener, The needle model: a new model for the main hydration peak of alite, Cem. Concr. Res. 115 (2019) 339–360, https://doi.org/10.1016/j.cemconres.2018.08.005.

[53] E.M.J. Bérodier, A.C.A. Muller, K.L. Scrivener, Effect of sulfate on C-S-H at early age, Cem. Concr. Res. 138 (2020), 106248, https://doi.org/10.1016/j.cemconres.2020.106248.

[54] H.M. Jennings, Refinements to colloid model of C-S-H in cement: CM-II, Cem. Concr. Res. 38 (2008) 275–289, https://doi.org/10.1016/j.cemconres.2007.10.006.

[55] J.J. De Yoreo, P.U.P.A. Gilbert, N.A.J.M. Sommerdijk, R.L. Penn, S. Whitelam, D. Joester, H. Zhang, J.D. Rimer, A. Navrotsky, J.F. Banfield, A.F. Wallace, F. M. Michel, F.C. Meldrum, H. Colfen, P.M. Dove, Crystallization by particle attachment in synthetic, biogenic, and geologic environments, Science 349 (2015), https://doi.org/10.1126/science.aaa6760 aaa6760–aaa6760.

[56] V.I. Kalikmanov, Classical nucleation theory, in: V.I. Kalikmanov (Ed.), Nucleation Theory, Springer, Netherlands, Dordrecht, 2013, pp. 17–41, https://doi.org/10.1007/978-90-481-3643-8_3.

[57] A.E.S. Van Driessche, L.G. Benning, J.D. Rodriguez-Blanco, M. Ossorio, P. Bots, J. M. García-Ruiz, The role and implications of bassanite as a stable precursor phase to gypsum precipitation, Science 336 (2012) 69–72, https://doi.org/10.1126/science.1215648.

[58] D. Li, M.H. Nielsen, J.R.I. Lee, C. Frandsen, J.F. Banfield, J.J. De Yoreo, Direction-specific interactions control crystal growth by oriented attachment, Science 336 (2012) 1014–1018, https://doi.org/10.1126/science.1219643.

[59] A.F. Wallace, L.O. Hedges, A. Fernandez-Martinez, P. Raiteri, J.D. Gale, G. A. Waychunas, S. Whitelam, J.F. Banfield, J.J. De Yoreo, Microscopic evidence for liquid-liquid separation in supersaturated CaCO3 solutions, Science 341 (2013) 885–889, https://doi.org/10.1126/science.1230915.

[60] A.I. Lupulescu, J.D. Rimer, In situ imaging of Silicalite-1 surface growth reveals the mechanism of crystallization, Science 344 (2014) 729–732, https://doi.org/10.1126/science.1250984.

[61] E. Pustovgar, R.P. Sangodkar, A.S. Andreev, M. Palacios, B.F. Chmelka, R.J. Flatt, J.-B. d'Espinose de Lacaillerie, Understanding silicate hydration from quantitative analyses of hydrating tricalcium silicates, Nat. Commun. 7 (2016) 10952, https://doi.org/10.1038/ncomms10952.

[62] A. Kumar, G. Sant, C. Patapy, C. Gianocca, K.L. Scrivener, The influence of sodium and potassium hydroxide on alite hydration: experiments and simulations, Cem. Concr. Res. 42 (2012) 1513–1523, https://doi.org/10.1016/j.cemconres.2012.07.003.

[63] J. Nehring, D. Jansen, J. Neubauer, F. Goetz-Neunhoeffer, Hydration of C3S in presence of CA : mineral-pore solution interaction, J. Am. Ceram. Soc. 102 (2019) 3152–3162, https://doi.org/10.1111/jace.16197.

[64] P. Suraneni, R.J. Flatt, Micro-reactors to study alite hydration, J. Am. Ceram. Soc. 98 (2015) 1634–1641, https://doi.org/10.1111/jace.13472.

[65] P. Suraneni, R.J. Flatt, Use of micro-reactors to obtain new insights into the factors influencing tricalcium silicate dissolution, Cem. Concr. Res. 78 (2015) 208–215, https://doi.org/10.1016/j.cemconres.2015.07.011.

[66] E. Pustovgar, R.K. Mishra, M. Palacios, J.-B. d'Espinose de Lacaillerie, T. Matschei, A.S. Andreev, H. Heinz, R. Verel, R.J. Flatt, Influence of aluminates on the hydration kinetics of tricalcium silicate, Cem. Concr. Res. 100 (2017) 245–262, https://doi.org/10.1016/j.cemconres.2017.06.006.

[67] B.R. Bickmore, K.L. Nagy, A.K. Gray, A.R. Brinkerhoff, The effect of Al(OH)4− on the dissolution rate of quartz, Geochim. Cosmochim. Acta 70 (2006) 290–305, https://doi.org/10.1016/j.gca.2005.09.017.

[68] D.V. Okhrimenko, C.F. Nielsen, L.Z. Lakshtanov, K.N. Dalby, D.B. Johansson, M. Solvang, J. Deubener, S.L.S. Stipp, Surface reactivity and dissolution properties of alumina-silica glasses and fibers, ACS Appl. Mater. Interfaces 12 (2020) 36740–36754, https://doi.org/10.1021/acsami.0c09362.

[69] F. Bellmann, H.-M. Ludwig, Analysis of aluminum concentrations in the pore solution during hydration of tricalcium silicate, Cem. Concr. Res. 95 (2017) 84–94, https://doi.org/10.1016/j.cemconres.2017.02.020.

[70] G. Mirabello, A. Ianiro, P.H.H. Bomans, T. Yoda, A. Arakaki, H. Friedrich, G. de With, N.A.J.M. Sommerdijk, Crystallization by particle attachment is a colloidal assembly process, Nat. Mater. 19 (2020) 391–396, https://doi.org/10.1038/s41563-019-0511-4.

[71] N. Krautwurst, L. Nicoleau, M. Dietzsch, I. Lieberwirth, C. Labbez, A. Fernandez-Martinez, A.E.S. Van Driessche, B. Barton, S. Leukel, W. Tremel, Two-step nucleation process of calcium silicate hydrate, the nanobrick of cement, Chem. Mater. 30 (2018) 2895–2904, https://doi.org/10.1021/acs.chemmater.7b04245.

[72] F. Bellmann, D. Damidot, B. Möser, J. Skibsted, Improved evidence for the existence of an intermediate phase during hydration of tricalcium silicate, Cem. Concr. Res. 40 (2010) 875–884, https://doi.org/10.1016/j.cemconres.2010.02.007.

[73] A.S. Brand, J.M. Gorham, J.W. Bullard, Dissolution rate spectra of β-dicalcium silicate in water of varying activity, Cem. Concr. Res. 118 (2019) 69–83, https://doi.org/10.1016/j.cemconres.2019.02.014.

[74] J.E. Rossen, B. Lothenbach, K.L. Scrivener, Composition of C-S–H in pastes with increasing levels of silica fume addition, Cem. Concr. Res. 9 (2015).

[75] A. Doroszkowski, The physical chemistry of dispersion, in: Paint Surf. Coat, Elsevier, 1999, pp. 198–242, https://doi.org/10.1533/9781855737006.198.

[76] D. Wagner, F. Bellmann, J. Neubauer, Influence of aluminium on the hydration of triclinic C3S with addition of KOH solution, Cem. Concr. Res. 137 (2020), 106198, https://doi.org/10.1016/j.cemconres.2020.106198.

[77] M. Boström, D.R.M. Williams, B.W. Ninham, Specific ion effects: why DLVO theory fails for biology and colloid systems, Phys. Rev. Lett. 87 (2001), 168103, https://doi.org/10.1103/PhysRevLett.87.168103.

[78] P.M. Dove, N. Han, Kinetics of mineral dissolution and growth as reciprocal microscopic surface processes across chemical driving force, in: AIP Conf. Proc, AIP, Park City, Utah (USA), 2007, pp. 215–234, https://doi.org/10.1063/1.2751917.

[79] E. Gartner, I. Maruyama, J. Chen, A new model for the C-S-H phase formed during the hydration of Portland cements, Cem. Concr. Res. 97 (2017) 95–106, https://doi.org/10.1016/j.cemconres.2017.03.001.

[80] J. Šefčík, A.V. McCormick, Thermochemistry of aqueous silicate solution precursors to ceramics, AIChE J. 43 (1997) 2773–2784.

[81] N.L. Thomas, J.D. Birchall, The retarding action of sugars on cement hydration, Cem. Concr. Res. 13 (1983) 830–842, https://doi.org/10.1016/0008-8846(83)90084-4.

[82] B. Lothenbach, G. Le Saout, M. Ben Haha, R. Figi, E. Wieland, Hydration of a low-alkali CEM III/B–SiO2 cement (LAC), Cem. Concr. Res. 42 (2012) 410–423, https://doi.org/10.1016/j.cemconres.2011.11.008.

[83] K. Yang, C.E. White, Modeling of aqueous species interaction energies prior to nucleation in cement-based gel systems, Cem. Concr. Res. 139 (2021), 106266, https://doi.org/10.1016/j.cemconres.2020.106266.

[84] N. Han, A.F. Wallace, Systematic dependence of kinetic and thermodynamic barriers to homogeneous silica nucleation on NaCl and amino acids, J. Mater. Res. 34 (2019) 442–455.

[85] H.F.W. Taylor , 11 admixtures and special uses of cements, in: Cem. Chem., n.d.: pp. 323–350. doi:10.1680/cc.25929.0011.

[86] H. Xu, J.S.J. Van Deventer, The geopolymerisation of alumino-silicate minerals, Int. J. Miner. Process. 59 (2000) 247–266, https://doi.org/10.1016/S0301-7516(99)00074-5.

[87] H. Matsuyama, J.F. Young, Effects of pH on precipitation of quasi-crystalline calcium silicate hydrate in aqueous solution, Adv. Cem. Res. 12 (2000) 29–33, https://doi.org/10.1680/adcr.2000.12.1.29.

[88] V. Kanchanason, J. Plank, Role of pH on the structure, composition and morphology of C-S-H–PCE nanocomposites and their effect on early strength development of Portland cement, Cem. Concr. Res. 102 (2017) 90–98, https://doi.org/10.1016/j.cemconres.2017.09.002.

[89] A.C. Lasaga, Transition state theory, Rev. Miner. States 8 (1981).

[90] P. Aagaard, H.C. Helgeson, Thermodynamic and kinetic constraints on reaction rates among minerals and aqueous solutions; I, theoretical considerations, Am. J. Sci. 282 (1982) 237, https://doi.org/10.2475/ajs.282.3.237.

[91] J. Schott, O.S. Pokrovsky, E.H. Oelkers, The link between mineral dissolution/precipitation kinetics and solution chemistry, Rev. Mineral. Geochem. 70 (2009) 207–258, https://doi.org/10.2138/rmg.2009.70.6.

[92] J. Plank, On the correct chemical nomenclature of C3S, tricalcium oxy silicate, Cem. Concr. Res. 130 (2020), 105957, https://doi.org/10.1016/j.cemconres.2019.105957.

[93] M.E. Tadros, J. Skalny, R.S. Kalyoncu, Early hydration of tricalcium silicate, J. Am. Ceram. Soc. 59 (1976) 344–347, https://doi.org/10.1111/j.1151-2916.1976.tb10980.x.

[94] E. Nägele, The zeta-potential of cement, Cem. Concr. Res. 15 (1985) 453–462.

[95] K. Suzuki, T. Nichikawa, K. Kato, H. Hayashi, S. Ito, Approach by zeta-potential measurement on the surface change of hydrating C3S, Cem. Concr. Res. 11 (1981) 759–764, https://doi.org/10.1016/0008-8846(81)90034-X.

[96] O. Galkin, P.G. Vekilov, Direct determination of the nucleation rates of protein crystals, J. Phys. Chem. B 103 (1999) 10965–10971, https://doi.org/10.1021/jp992786x.

[97] B. Fritz, C. Noguera, Mineral precipitation kinetics, Rev. Mineral. Geochem. 70 (2009) 371–410, https://doi.org/10.2138/rmg.2009.70.8.
[98] A.F. Wallace, J.J. DeYoreo, P.M. Dove, Kinetics of silica nucleation on carboxyl- and amine-terminated surfaces: insights for biomineralization, J. Am. Chem. Soc. 131 (2009) 5244–5250, https://doi.org/10.1021/ja809486b.
[99] C. Ratsch, J.A. Venables, Nucleation theory and the early stages of thin film growth, J. Vac. Sci. Technol. Vac. Surf. Films 21 (2003) S96–S109, https://doi.org/10.1116/1.1600454.
[100] M. Schönlein, J. Plank, A TEM study on the very early crystallization of C-S-H in the presence of polycarboxylate superplasticizers: transformation from initial C-S-H globules to nanofoils, Cem. Concr. Res. 106 (2018) 33–39, https://doi.org/10.1016/j.cemconres.2018.01.017.
[101] H.M. Jennings, Aqueous solubility relationships for two types of calcium silicate hydrate, J. Am. Ceram. Soc. 69 (1986) 614–618, https://doi.org/10.1111/j.1151-2916.1986.tb04818.x.
[102] F. Deschner, F. Winnefeld, B. Lothenbach, S. Seufert, P. Schwesig, S. Dittrich, F. Goetz-Neunhoeffer, J. Neubauer, Hydration of Portland cement with high replacement by siliceous fly ash, Cem. Concr. Res. 42 (2012) 1389–1400, https://doi.org/10.1016/j.cemconres.2012.06.009.
[103] C. Nalet, A. Nonat, Ionic complexation and adsorption of small organic molecules on calcium silicate hydrate: relation with their retarding effect on the hydration of C3S, Cem. Concr. Res. 89 (2016) 97–108, https://doi.org/10.1016/j.cemconres.2016.08.012.
[104] M.R. Andalibi, A. Kumar, B. Srinivasan, P. Bowen, K. Scrivener, C. Ludwig, A. Testino, On the mesoscale mechanism of synthetic calcium–silicate–hydrate precipitation: a population balance modeling approach, J. Mater. Chem. A 6 (2018) 363–373, https://doi.org/10.1039/C7TA08784E.
[105] A.J. Allen, J.J. Thomas, Analysis of C-S–H gel and cement paste by small-angle neutron scattering, Cem. Concr. Res. 37 (2007) 319–324, https://doi.org/10.1016/j.cemconres.2006.09.002.